NASA Technical Memorandum 4037

BRYNTRN: A Baryon Transport Computer Code

Computation Procedures and Data Base

John W. Wilson, Lawrence W. Townsend,
Sang Y. Chun, Warren W. Buck,
Ferdous Khan, and Frank Cucinotta

JUNE 1988

NASA

NASA Technical Memorandum 4037

BRYNTRN: A Baryon Transport Computer Code

Computation Procedures and Data Base

John W. Wilson and Lawrence W. Townsend
Langley Research Center
Hampton, Virginia

Sang Y. Chun and Warren W. Buck
Hampton University
Hampton, Virginia

Ferdous Khan and Frank Cucinotta
Old Dominion University
Norfolk, Virginia

National Aeronautics
and Space Administration

**Scientific and Technical
Information Division**

1988

Abstract

The present report describes the development of an interaction data base and a numerical solution to the transport of baryons through an arbitrary shield material based on a straight ahead approximation of the Boltzmann equation. The code is most accurate for continuous energy boundary values but gives reasonable results for discrete spectra at the boundary with even a relatively coarse energy grid (30 points) and large spatial increments (1 cm in H_2O).

1. Introduction

The purpose of the present report is to describe computer programs developed for the calculation of the transport of high energy nucleons (baryons) and their interaction with materials. The methods, based on the direct solution of the Boltzmann equation, have been developed over the last several years (refs. 1–4). The solutions employ the straight ahead approximations for which energy changing processes are accurately handled, but all propagation occurs along a fixed direction. The present goal is to document a relatively complete description of the basic physical processes even though the input data base used requires some improvement. Future work will concentrate on improving the data base, code efficiency, and the computational procedures.

2. Theoretical Considerations

2.1. Boltzmann Equation

The equations in the straight ahead approximation to be solved (ref. 5) are

$$\left[\frac{\partial}{\partial x} - \frac{\partial}{\partial E}S(E) + \sigma_p(E)\right] \phi_p(x,E) = \sum_j \int_E^\infty f_{pj}(E,E')\ \phi_j(x,E')\ dE' \tag{2.1.1}$$

$$\left[\frac{\partial}{\partial x} + \sigma_n(E)\right] \phi_n(x,E) = \sum_j \int_E^\infty f_{nj}(E,E')\ \phi_j(x,E')\ dE' \tag{2.1.2}$$

where $\phi_j(x,E)$ is the type j particle differential flux density at x with energy E; $S(E)$ is proton stopping power; $\sigma_p(E)$, $\sigma_n(E)$ are proton, neutron total cross section, respectively; and $f_{ij}(E,E')$ are the differential cross sections for elastic and nonelastic processes. New field quantities are conveniently defined as

$$r = \int_0^E dE'/S(E') \tag{2.1.3}$$

$$\psi_j(x,r) = S(E)\phi_j(x,E) \tag{2.1.4}$$

$$\bar{f}_{ij}(r,r') = S(E)f_{ij}(E,E') \tag{2.1.5}$$

so that

$$\left[\frac{\partial}{\partial x} - \frac{\partial}{\partial r} + \sigma_p(r)\right] \psi_p(x,r) = \sum_j \int_r^\infty \bar{f}_{pj}(r,r')\ \psi_j(x,r')\ dr' \tag{2.1.6}$$

$$\left[\frac{\partial}{\partial x} + \sigma_n(r)\right] \psi_n(x,r) = \sum_j \int_r^\infty \bar{f}_{nj}(r,r')\ \psi_j(x,r')\ dr' \tag{2.1.7}$$

which can be rewritten as integral equations with boundary at $x = 0$. The results follow:

$$\psi_p(x,r) = e^{-\int_0^x \sigma_p(r+z)\,dz}\psi_p(0,r+x) + \int_0^x dz\; e^{-\int_0^z \sigma_p(r+w)\,dw} \sum_j \int_{r+z}^{\infty} \bar{f}_{pj}(r+z,r')\;\psi_j(x-z,r')\;dr' \tag{2.1.8}$$

$$\psi_n(x,r) = e^{-\sigma_n(r)x}\psi_n(0,r) + \int_0^x dz\; e^{-\sigma_n(r)z} \sum_j \int_r^{\infty} \bar{f}_{nj}(r,r')\;\psi_j(x-z,r')\;dr' \tag{2.1.9}$$

These equations relate the known flux at the boundary at $x = 0$ to an interior point. We choose the point to be $x = h$, where h is a small distance, and write

$$\psi_p(x+h,r) = e^{-\int_0^h \sigma_p(r+w)\,dw}\psi_p(x,r+h) + \int_0^h dz\; e^{-\int_0^z \sigma_p(r+w)\,dw} \sum_j \int_{r+z}^{\infty} \bar{f}_{pj}(r+z,r')\;\psi_j(x+h-z,r')\;dr' \tag{2.1.10}$$

$$\psi_n(x+h,r) = e^{-\sigma_n(r)h}\psi_n(x,r) + \int_0^h dz\; e^{-\sigma_n(r)z} \sum_j \int_r^{\infty} \bar{f}_{nj}(r,r')\;\psi_j(x+h-z,r')\;dr \tag{2.1.11}$$

To evaluate equations (2.1.10) and (2.1.11), the flux $\psi_j(x,r)$ is required across the interval. This we do as follows:

If h is sufficiently small such that

$$\sigma_j(r')h \ll 1 \tag{2.1.12}$$

then according to perturbation theory (ref. 1)

$$\psi_p(x+h-z,r') \approx e^{-\int_0^{h-z} \sigma_p(r'+w)\,dw}\psi_p(x,r'+h-z) \tag{2.1.13}$$

$$\psi_n(x+h-z,r') \approx e^{-\sigma_n(r')(h-z)}\psi_n(x,r') \tag{2.1.14}$$

which may be used to approximate the above integrals of equations (2.1.10) and (2.1.11).

For many cases of practical interest (e.g., accelerator studies), monoenergetic particle beams are used, and separation of the singular terms from the solution becomes convenient. The initial beam of type J particles of energy $E_0(r_0 = R(E_0))$ is taken as

$$\psi_j(0,r) = \delta_{jJ}\delta(r_0 - r) \tag{2.1.15}$$

and the solution is written as

$$\psi_j(x,r) = \psi_{j0}(x,r) + \psi_j(x,r) \tag{2.1.16}$$

The corresponding singular terms are

$$\psi_{p0}(x,r) = e^{-\int_0^x \sigma_p(r+w)\,dw}\delta(r_0 - r - x)\delta_{pj} \tag{2.1.17}$$

$$\psi_{n0}(x,r) = e^{-\sigma_n(r)x}\delta(r_0 - r)\delta_{nj} \tag{2.1.18}$$

The regular terms of equations (2.1.10) and (2.1.11) may be written as

$$\psi_p(x+h,r) = e^{-\int_0^h \sigma_p(r+w)\,dw}\psi_p(x,r+h) + \int_0^h dz\; e^{-\int_0^z \sigma_p(r+w)\,dw} \times \sum_j \int_{r+z}^{\infty} \bar{f}_{pj}(r+z,r')\left[\psi_{j0}(x+h-z,r') + \psi_j(x+h-z,r')\right] dr' \qquad (2.1.19)$$

$$\psi_n(x+h,r) = e^{-\sigma_n(r)h}\psi_n(x,r) + \int_0^h dz\; e^{-\sigma_n(r)z} \times \sum_j \int_r^{\infty} \bar{f}_{nj}(r,r')\left[\psi_{j0}(x+h-z,r') + \psi_j(x+h-z,r')\right] dr' \qquad (2.1.20)$$

The singular contributions under the integrals of equations (2.1.19) and (2.1.20) can be evaluated with equations (2.1.17) and (2.1.18) and the approximations (2.1.12)–(2.1.14) applied to find

$$\begin{aligned}\psi_p(x+h,r) = {} & e^{-\sigma_p(r)h}\psi_p(x,r+h) \\ & + e^{-[\sigma_p(r)+\sigma_p(r_0')]\frac{h}{2}}\bar{F}_{pp}(h,r,r_0')\delta_{pj}e^{-\int_0^x \sigma_p(r_0'+w)\,dw} \\ & + e^{-[\sigma_p(r)+\sigma_n(r_0)]\frac{h}{2}}\bar{F}_{pn}(h,r,r_0)\delta_{nj}e^{-\sigma_n(r_0)x} \\ & + \int_r^{\infty} e^{-\left[\sigma_p(r)+\sigma_p\left(r'+\frac{h}{2}\right)\right]\frac{h}{2}}\bar{F}_{pp}\left(h,r,r'+\frac{h}{2}\right)\psi_p(x,r'+h)\,dr' \\ & + \int_r^{\infty} e^{-\left[\sigma_p(r)+\sigma_n\left(r'+\frac{h}{2}\right)\right]\frac{h}{2}}\bar{F}_{pn}\left(h,r,r'+\frac{h}{2}\right)\psi_n(x,r'+h)\,dr' \end{aligned} \qquad (2.1.21)$$

and

$$\begin{aligned}\psi_n(x+h,r) = {} & e^{-\sigma_n(r)h}\psi_n(x,r) \\ & + h\bar{f}_{np}(r,r_0')e^{-[\sigma_n(r)+\sigma_p(r_0')]\frac{h}{2}}\delta_{pj}e^{-\int_0^x \sigma_p(r_0'+w)\,dw} \\ & + h\bar{f}_{nn}(r,r_0)e^{-[\sigma_n(r)+\sigma_n(r_0)]\frac{h}{2}}\delta_{nj}e^{-\sigma_n(r_0)x} \\ & + h\int_r^{\infty} e^{-[\sigma_n(r)+\sigma_p(r')]\frac{h}{2}}\bar{f}_{np}(r,r')\;\psi_p\left(x,r'+\frac{h}{2}\right)dr' \\ & + h\int_r^{\infty} e^{-[\sigma_n(r)+\sigma_n(r')]\frac{h}{2}}\bar{f}_{nn}(r,r')\;\psi_n(x,r')\,dr' \end{aligned} \qquad (2.1.22)$$

where $r_0' = r_0 - x - \frac{h}{2}$ and $\bar{F}$ is related to the cumulative spectrum F as

$$\begin{aligned}\bar{F}_{ij}(h,r,r') &= \int_0^{\infty} \bar{f}_{ij}(r+z,r')\,dz \\ &= F_{ij}(r+h,r') - F_{ij}(r,r') \end{aligned} \qquad (2.1.23)$$

with

$$F_{ij}(r,r') = \int_0^{\epsilon(r)} f_{ij}(E,E')\,dE \qquad (2.1.24)$$

and $\epsilon(r)$ is the energy associated with residual range r, and $E' = \epsilon(r')$. Equations (2.1.20) and (2.1.21) are evaluated by establishing an x-grid at which $\psi_j(x_m, r)$ is evaluated, and h is the distance between each successive evaluation. The integral over r' is accomplished by establishing an r-grid (and the corresponding E-grid) and using

$$\int_{r_n}^{\infty} g(r_n, r')\psi_j(x_m, r')\, dr'$$

$$\approx \sum_{\ell=n}^{\infty} g_n(r_n, \bar{r}_\ell) \int_{r_\ell}^{r_{\ell+1}} \psi_j(x_m, r')\, dr' \tag{2.1.25}$$

where $\bar{r}_\ell = (r_\ell + r_{\ell+1})/2$, and the series terminates at the highest ℓ value in the r-grid. There is a spatially dependent discontinuity in the proton flux spectrum that requires right- and left-hand interpolation and integration. These discontinuities have been treated in the computational procedures.

2.2. Neutron Source

The neutron transport equation in three dimensions is

$$\left[\vec{\Omega} \cdot \nabla + \sigma_n(E)\right] \phi_n(\vec{x}, \vec{\Omega}, E) = \sum_j \int_E^{\infty} f_{nj}(E, E', \vec{\Omega}, \vec{\Omega}')\, \phi_j(\vec{x}, \vec{\Omega}', E')\, d\Omega'\, dE' \tag{2.2.1}$$

While it is true that the straight ahead approximation is adequate for most proton calculations, the neutron fields are more strongly affected by non-forward scattering components, particularly the low energy neutrons. The reason is that the lower energy neutrons have a greater range than lower energy protons because of the electric charge difference. Thus, a first-order correction to the straight ahead approximation may be applied by substituting the proton coupling in equation (2.2.1) by the straight ahead solution for $\phi_p(\vec{x}, \vec{\Omega}, E)$ so that

$$\xi_n(\vec{x}, \vec{\Omega}, E) = \int_E^{\infty} f_{np}(E, E', \vec{\Omega}, \vec{\Omega}_x)\, \phi_p(\vec{x}, E')\, dE' \tag{2.2.2}$$

The corresponding neutron transport equation is

$$\left[\vec{\Omega} \cdot \nabla + \sigma_n(E)\right] \phi_n(\vec{x}, \vec{\Omega}, E) = \int_E^{\infty} f_{nn}(E, E', \vec{\Omega}, \vec{\Omega}')\, \phi_n(\vec{x}, \vec{\Omega}', E')\, d\Omega'\, dE' + \xi_n(\vec{x}, \vec{\Omega}, E) \tag{2.2.3}$$

The neutron source integral is evaluated in a fashion similar to equation (2.1.25).

2.3. Target Fragment Secondary Flux

The target fragmentations produced in nuclear collision with the nucleon field must now be treated. The spectral parameters of the composite fragments are relatively independent of the projectile charge, energy, or direction. This leads to some simplifying assumptions so that

$$\phi_j^T(\vec{x}, \vec{\Omega}, E) = \frac{1}{S_j(E)} \xi_j(\vec{x}) \int_E^{E\gamma} f_j(E')\, dE' \tag{2.3.1}$$

$$E\gamma = R_j^{-1}\left[R_j(E) + d(\vec{\Omega})\right] \tag{2.3.2}$$

where $d(\vec{\Omega})$ is the distance from the boundary (ref. 2). The source of ions of type j is evaluated as

$$\xi_j(\vec{x}) = \sum_i \int_0^{\infty} \sigma_{ji}(E')\, \phi_i(\vec{x}, \vec{\Omega}', E')\, d\vec{\Omega}'\, dE' \tag{2.3.3}$$

where $\sigma_{ji}(E)$ are the fragmentation cross sections. The term $f_j(E)$ represents the spectral contributions averaged over all the target atomic constituents. In the present code, the distance to the boundary is assumed large. One could treat not only boundary effects but interface effects as well.

3. Transport Coefficients

3.1. Stopping Power

In passing through a material, an ion loses the larger fraction of its energy to electronic excitation of the material. Although a satisfactory theory of high-energy ion-electron interaction is available in the form of Bethe's theory utilizing the Born approximation, an equally satisfactory theory for low energies is not available. Bethe's high-energy approximation to the energy loss per unit path (that is, stopping power) is given as

$$S_e = \frac{4\pi N Z_1^2 Z_2 e^4}{mv^2} \left\{ \ln \left[\frac{2mv^2}{(1-\beta^2)I_2} \right] - \beta^2 - \frac{C}{Z_2} \right\} \tag{3.1.1}$$

where Z_1 is the projectile charge, N is the number of target molecules per unit volume, Z_2 is the number of electrons per target molecule, m is the electron mass, v is the projectile velocity, $\beta = v/c$, c is the velocity of light, C is the velocity-dependent shell correction term (ref. 6), and I_2 is the mean excitation energy given by

$$Z_2 \ln(I_2) = \sum_n f_n \ln(E_n) \tag{3.1.2}$$

where f_n are the electric dipole oscillator strengths of the target and E_n are the corresponding excitation energies. Note that the sum in equation (3.1.2) includes discrete and continuum levels. Molecular stopping power is reasonably approximated by the sum of the corresponding empirically derived "atomic" stopping powers for which equations (3.1.1) and (3.1.2) imply that

$$Z \ln(I) = \sum_j n_j Z_j \ln(I_j) \tag{3.1.3}$$

where Z and I pertain to the molecule, Z_j and I_j are the corresponding atomic values, and n_j are the stoichiometric coefficients. This additive rule (eq. (3.1.3)) is usually called Bragg's rule (ref. 7).

Sources of deviations from Bragg's additive rule for molecules and for the condensed phase are discussed by Platzman (ref. 8). Aside from shifts in excitation energies and adjustments in line strengths as a result of molecular bonding, new terms in the stopping power appear due to coupling between vibrational and rotational modes. Additionally, in the condensed phase, some discrete transitions are moved into the continuum, and collective modes among valence electrons in adjacent atoms produce new terms in the absorption spectrum to be dealt with. Platzman proposed that the experimentally observed additivity rule may not show that molecular stopping power is the sum of atomic processes, but rather demonstrates that molecular bond shifts for covalent bonded molecules are relatively independent of the molecular combination. On the basis of such arguments, Platzman suggested that ionic bonded substances should be studied as a rigid test of the additive rule because of the radical difference in bonding type. He further estimated that ionic bond shifts could change the stopping power by as much as 50 percent. Recent results on shifts of mean excitation energies due to molecular bonds are discussed in references 9 to 11. Effects of the physical state have likewise been studied (ref. 12).

The electronic stopping power for protons is adequately described by equation (3.1.1) for energies above 500 keV for which the shell or "tight binding" correction C makes an important contribution below 10 MeV (ref. 13). For proton energies below 500 keV, charge exchange (electron transfer) reactions alter the proton charge over much of its path, so that equation (3.1.1) is to be understood in terms of an average over the proton charge states.

Normally an average over the charge states is introduced into equation (3.1.1) so that the effective charge is the root-mean-square ion charge and not the average ion charge. At any ion energy, charge equilibrium is established very quickly in all materials. Utilizing the effective charge in equation (3.1.1) appears to make only modest improvement below 500 keV, an indication presumably of the failure of this theory based on an empirical basis (refs. 13 and 14). The resultant stopping power for protons in water is shown in comparison with the evaluated data of Bichsel (ref. 15) in figure 1.

The electronic stopping power for alpha particles requires terms in equation (3.1.1) of higher order in the projectile charge Z_1 because of corrections to the Born approximation. The alpha stopping power cannot be related to the proton stopping power through their effective charges. Parametric fits to experimental data are given by Ziegler in reference 16 for all elements in both the gaseous and the condensed phases.

The electronic stopping powers for heavier ions are related to the alpha stopping power through their corresponding effective charges. The effective charge suggested by Barkas (ref. 17) is used:

$$Z^{\star} = Z\left[1 - \exp\left(-125\beta/Z^{2/3}\right)\right] \tag{3.1.4}$$

where Z in equation (3.1.4) is the atomic number of the ion.

At sufficiently low energies, the energy lost by an ion in a nuclear collision becomes important. The nuclear stopping theory used in this paper is a modification of the theory of Lindhard, Scharff, and Schiott (ref. 18). The reduced energy is given as

$$\epsilon = \frac{32.53 A_1 A_2 E}{Z_1 Z_2 (A_1 + A_2)\left(Z_1^{2/3} + Z_2^{2/3}\right)^{1/2}} \tag{3.1.5}$$

where E is in units of keV/nucleon, and A_1 and A_2 are the atomic masses of the projectile and the target. The nuclear stopping power in reduced units (ref. 16) is

$$S_n = \begin{cases} 1.59\epsilon^{1/2} & (\epsilon < 0.01) \\ \dfrac{1.7\epsilon^{1/2}\ \ln(\epsilon + \exp 1)}{1 + 6.8\epsilon + 3.4\epsilon^{3/2}} & (0.01 < \epsilon < 10) \\ \dfrac{\ln(0.47\epsilon)}{2\epsilon} & (\epsilon > 10) \end{cases} \tag{3.1.6}$$

and the conversion factor to units of $\mathrm{eV}/10^{15}$ atoms/cm^2 is

$$f = \frac{8.426 Z_1 A_2 A_1}{(A_1 + A_2)\left(Z_1^{2/3} + Z_2^{2/3}\right)^{1/2}} \tag{3.1.7}$$

The total stopping power S_j is obtained by summing the electronic and nuclear contributions. Other processes of energy transfer such as Bremsstrahlung and pair production are unimportant.

For energies above a few MeV/nucleon, Bethe's equation is adequate provided that appropriate corrections to Bragg's rule (refs. 9 to 11), shell corrections (refs. 6, 13, and 14), and an effective charge are included. Electronic stopping power for protons is calculated from the parametric formulas of Andersen and Ziegler (ref. 13). The calculated stopping power for protons in water is shown in figure 1 in comparison with data given by Bichsel (ref. 15).

Because alpha stopping power is not derivable from the proton stopping power formula by using the effective charge at low energy, the parametric fits to empirical alpha stopping powers given by Ziegler (ref. 16) are used. Applying his results for condensed phase water poorly represented the data of references 19 and 20. Considering that physical state and molecular binding effects are most important for hydrogen (ref. 9), the water stopping power

was approximated by using the condensed phase parameters for hydrogen and the gas phase parameters for oxygen (which are known experimentally). These results are compared with experimental data for condensed phase water (refs. 19 and 20) in figure 1. It appears that Ziegler overestimated the condensed phase effects for oxygen since the gas phase oxygen data give satisfactory results as seen in figure 1.

Electronic stopping powers for ions with a charge greater than 2 are related to the alpha stopping power through the effective charge given by equation (3.1.4). For water, the condensed phase formula of Ziegler for alpha particles gives probably the best stopping powers for heavier ions. Calculated results for ^{16}O and ^{56}Fe ions in water are shown in figure 1 in comparison with the Northcliffe and Schilling data (ref. 21). Good agreement with Northcliffe and Schilling for ^{56}Fe ions is especially important since their data seem to agree with the range experiments of J. H. Chan in Lexan resin (ref. 22). The stopping powers in Lexan resin and tissue equivalent material can be calculated in a way similar to the procedure given above for calculating stopping powers in water.

3.2. Nuclear Absorption Cross Sections

The nuclear absorption cross sections are calculated using a parameterization obtained by fitting an analytical expression to experimental data. For nucleon-nucleus collisions, it is given in millibarns by (ref. 23)

$$\sigma_A = f(E)45A^{0.7}\{1 + 0.016\ \sin[5.3 - 2.63\ \ln(A)]\} \tag{3.2.1}$$

where A is the mass number of the target nucleus, and the energy-dependent factor is

$$f(E) = 1 - 0.62e^{-E/200}\sin\left(10.9E^{-0.28}\right) \tag{3.2.2}$$

with the incident kinetic energy E in units of MeV/nucleon.

3.3. Total Nuclear Cross Sections

The proton-proton (pp) total cross section is found to be approximately

$$\sigma_{pp}(E) = (1 + 5/E)\left[40 + 109\ \cos(0.199\sqrt{E})\right]e^{-.451(E-25)^{.258}} \tag{3.3.1}$$

for $E \geq 25$ MeV and taken as

$$\sigma_{pp}(E) = e^{6.51e^{-(E/134)^{.7}}} \tag{3.3.2}$$

at lower energies. The neutron-proton (np) cross section is taken as

$$\sigma_{np}(E) = 38 + 12500e^{-1.187(E-.1)^{.35}} \tag{3.3.3}$$

which is used for $E \geq 0.1$ MeV and taken as

$$\sigma_{np}(E) = 26000e^{-(E/.282)^{.3}} \tag{3.3.4}$$

at lower energies.

The low energy neutron-nucleus cross sections exhibit a complicated resonance structure over a nearly constant background. Above 20 MeV, the cross sections decrease with energy to

a minimum at 300 MeV and rise slightly to 1 GeV and remain nearly constant thereafter. In the present code, the total neutron cross sections are approximated at four energies as

$$\sigma_t(E,A) = \left\{ \begin{array}{ll} 0.3A^{.656} + 0.5Ae^{-0.066A} & (E = 0.1 \text{ MeV}) \\ 0.38A^{.525} + 0.09Ae^{-.05A} & (E = 1.5 \text{ MeV}) \\ 0.45A^{.475} + 0.025Ae^{-.06A} & (E = 20 \text{ MeV}) \\ 0.052A^{.726} + 0.02Ae^{-.025A} & (E = 100 \text{ MeV}) \end{array} \right\} \tag{3.3.5}$$

These are extended to lower and higher energies and interpolated using

$$\sigma(E,A) = \sigma(E_i,A)e^{-a(E-E_i)} \tag{3.3.6}$$

where $\sigma(E_i,A)$ is the appropriate cross section at one of the above energies and a is determined to ensure appropriate interpolation or extrapolation. This quantity is used to calculate the scattering cross section as

$$\sigma_s(E) = \sigma_{\text{tot}}(E) - \sigma_{\text{abs}}(E) \tag{3.3.7}$$

used for $\sigma_{\text{tot}}(E) > 2\sigma_{\text{abs}}(E)$, which occurs for values of E less than or about 200 MeV and

$$\sigma_s(E) = \sigma_{\text{abs}}(E) \tag{3.3.8}$$

otherwise.

The total neutron-nucleus cross section is shown in comparison with experimental data (ref. 24) in figures 2 to 4 (data shown as the solid curve) and in table 3.3.1. These functions should be improved in future work.

3.4. Fragmentation Cross Sections

The nuclear cross section for producing fragment A_f, Z_f from a target A_t, Z_t is taken from Rudstam (ref. 25) as

$$\sigma(A_f,Z_f) = \frac{F_1F_2pA_t^{-0.3}e^{-\left(pA_f - r\left|Z_f - SA_f + VA_f^2\right|^{1.5}\right)}}{D} \tag{3.4.1}$$

where

$$D = 1.79\left[e^{pA_t}\left(1 - \frac{0.3}{pA_t}\right) - \frac{0.3}{A_t} + \frac{0.3}{pA_t}\right] \tag{3.4.2}$$

$$F_1 = 11.8^{2/3}e^{-G+HA_t} \tag{3.4.3}$$

$$F_2 = \left\{ \begin{array}{ll} e^{K-LE} & (E < 240 \text{ MeV}) \\ 1.0 & (E \geq 240 \text{ MeV}) \end{array} \right\} \tag{3.4.4}$$

$$p = \left\{ \begin{array}{ll} 20E^{-.77} & (E < 2100 \text{ MeV}) \\ 0.056 & (E \geq 2100 \text{ MeV}) \end{array} \right\} \tag{3.4.5}$$

$$r = 11.8A_f^{-0.45} \tag{3.4.6}$$

$$S = 0.486 \tag{3.4.7}$$

$$V = 3.8 \times 10^{-4} \tag{3.4.8}$$

$$G = 0.25 \tag{3.4.9}$$

$$H = 0.0074 \tag{3.4.10}$$

$$K = 1.73 \tag{3.4.11}$$

$$L = 0.0071 \tag{3.4.12}$$

Correction factors for ^{12}C and ^{16}O fragments are given in table 3.4.1. The total of all fragmentations is renormalized to the total absorption cross section at each energy. The major isotope fragments are reasonably well produced for light to medium-heavy fragments. Many other corrections to the basic Rudstam formalism have been made by Silberberg and Tsao (ref. 26).

3.5. Differential Nuclear Cross Sections

3.5.1. Nucleon-nucleon spectrum. The nucleon-nucleon differential cross sections are represented (ref. 27) by

$$f(E,E') = B\left[e^{-B(E'-E)} + e^{-BE}\right] \Big/ \left(1 - e^{-BE'}\right) \tag{3.5.1}$$

where

$$B = 2mc^2 b/10^6 \tag{3.5.2}$$

In the above, mc^2 is the nucleon rest energy (938 MeV) and b is the usual slope parameter, given by (units of GeV^{-2})

$$b = \left\{ \begin{array}{ll} 3 + 14e^{-E'/200} & (\text{for } pp) \\ 3.5 + 30e^{-E'/200} & (\text{for } np) \end{array} \right\} \tag{3.5.3}$$

where E' is the initial nucleon energy in the rest frame of the target. The differential spectrum is defined (nonrelativistically) over the energy interval $0 \leq E \leq E'$. Note that the expression (3.5.1) reduces to the usual result for low energy scattering

$$f(E,E') \approx 1/E' \tag{3.5.4}$$

The forward to backward scattering ratio is required for neutron scattering and is given by (ref. 28)

$$F_B(E') = 0.12 - .015E' + \frac{0.41}{1 + e^{4(E'-2.1)}} \tag{3.5.5}$$

where E' in equation (3.5.5) is the laboratory energy in GeV before collision.

The differential cross sections are normalized such that

$$\frac{d\sigma}{dE} = \sigma(E')\ f(E,E') \tag{3.5.6}$$

where $\sigma(E')$ is the appropriate nucleon-nucleon total cross section. Obviously we have neglected the inelastic processes, which must yet be included. The center of mass angular distributions (θ_{cm}) are related to the energy change in the laboratory system by

$$\frac{d\sigma}{d\Omega} = \frac{E'}{4\pi}\frac{d\sigma}{dE} \tag{3.5.7}$$

and are compared with the compilation of experimental data (ref. 29) in figures 5 and 6. These comparisons indicate that the present functions are reasonable.

3.5.2. Nucleon-nucleus spectrum. The nucleon-nucleus differential cross section in the impulse (Chew) approximation (note, this is just the Born term of the optical model, ref. 30) is given by

$$\frac{d\sigma}{dq^2} = ce^{-2bq^2}|F_A(q^2)|^2 \approx ce^{-2bq^2}e^{-2a^2q^2/3} \tag{3.5.8}$$

where b is the slope parameter of equation (3.5.2) averaged among nuclear constituents, q is the magnitude of momentum transfer, and a is the nuclear rms radius. The nuclear rms radius in terms of the rms charge radius in fm is given as

$$a = \sqrt{a_c^2 - 0.64} \tag{3.5.9}$$

where the rms charge radius in fm is

$$a_c = \left\{ \begin{array}{ll} 0.84 & (A_t = 1) \\ 2.17 & (A_t = 2) \\ 1.78 & (A_t = 3) \\ 1.63 & (A_t = 4) \\ 2.4 & (6 \leq A_t \leq 14) \\ 0.82A_t^{1/3} + 0.58 & (A_t \geq 16) \end{array} \right\} \tag{3.5.10}$$

The nuclear form factor is the Fourier transform of the nuclear matter distribution. Note that the above assumes the nuclear matter distribution is a Gaussian function, which is reasonable for the light mass nuclei but is less valid for $A_t >> 20$.

The energy transferred to the nucleus E_t is restricted by kinematics to

$$0 \leq E_t \leq (1 - \alpha)E' \tag{3.5.11}$$

where

$$\alpha = \frac{(A_t - 1)^2}{(A_t + 1)^2} \tag{3.5.12}$$

The energy transfer spectrum is given as

$$f(E_t, E') = \frac{4A_tmc^2(B + a^2/3)e^{-4A_tmc^2(B+a^2/3)E_t}}{\left[1 - e^{-4A_tmc^2(1-\alpha)(B+a^2/3)E'}\right]} \tag{3.5.13}$$

Similarly, the nucleon energy after scattering E is restricted to

$$\alpha E' \leq E \leq E' \tag{3.5.14}$$

The nucleon spectrum is given by

$$f(E, E') = \frac{4A_tmc^2(B + a^2/3)e^{-4A_tmc^2(B+a^2/3)(E'-E)}}{\left[1 - e^{-4A_tmc^2(1-\alpha)(B+a^2/3)E'}\right]} \tag{3.5.15}$$

One should note that both equations (3.5.13) and (3.5.15) reduce to the usual isotropic scattering result at low incident energy.

The results of equation (3.5.15) are compared with experiment (refs. 31 and 32) in figures 7 to 10. The comparison is rather good at the small angles, considering the simplicity of the present results, but there is definite room for improvement. Much of the present discrepancy is due to errors in $\sigma_s(E)$ to which the present spectra are normalized in equation (3.5.7).

3.5.3. Nucleon nonelastic spectrum. The nonelastic differential cross sections use the results of Bertini's MECC7 program. The nucleon multiplicities are given in tables 3.5.1 and 3.5.2. We have required the multiplicities to be monotonic in energy so the values in parentheses are corrected values obtained by scaling from lower and higher energies and are used in the calculations. The results below 400 MeV were taken from Alsmiller et al. (ref. 33), and the results for carbon, calcium, bromine cesium, and holmium above 400 MeV are obtained by interpolation. The nonelastic spectra are represented as

$$f(E,E') = \sum_{i=1}^{3} \frac{N_i}{\alpha_i} \frac{e^{-E/\alpha_i}}{1-e^{-E'/\alpha_i}} + \frac{N_Q}{E'\left[1+e^{-20(1-E/E')}\right]} \tag{3.5.16}$$

The first term of the summation represents the evaporation peak so that N_1 is taken from table 3.5.1 and the spectral parameter α_1 (GeV) is taken from Ranft (ref. 34) as

$$\alpha_{1_p} = \left\{ \begin{array}{ll} (0.019+0.0017E')(1-0.001A_t) & (E' < 5 \text{ GeV}) \\ 0.027(1-0.001A_t) & (E' \geq 5 \text{ GeV}) \end{array} \right\} \tag{3.5.17}$$

$$\alpha_{1_n} = \left\{ \begin{array}{ll} (0.017+0.0017E')(1-0.001A_t) & (E' < 5 \text{ GeV}) \\ 0.023(1-0.001A_t) & (E' \geq 5 \text{ GeV}) \end{array} \right\} \tag{3.5.18}$$

The second term is taken from Ranft (ref. 34) to represent the low energy cascade particles as

$$n_{2p} = \left\{ \begin{array}{ll} 0.0035\sqrt{A_t} & (E' \leq 0.1 \text{ GeV}) \\ 0.007\sqrt{A_t}\left[0.5+(1+\log_0 E')^2\right] & (0.1 < E' < 5 \text{ GeV}) \\ 0.0245\sqrt{A_t} & (E' \geq 5) \end{array} \right\} \tag{3.5.19}$$

$$n_{2n} = \left\{ \begin{array}{ll} 0.0042\sqrt{A_t} & (E' \leq 0.1 \text{ GeV}) \\ 0.007\sqrt{A_t}\left[0.6+1.3(1+\log_{10} E')^2\right] & (0.1 < E' < 5 \text{ GeV}) \\ 0.032\sqrt{A_t} & (E' \geq 5 \text{ GeV}) \end{array} \right\} \tag{3.5.20}$$

with the corresponding spectral parameters

$$\left. \begin{array}{l} \alpha_{2p} = \left\{ \begin{array}{ll} (0.11+0.01E')\ (1-0.001A_t) & (E' < 5 \text{ GeV}) \\ 0.16(1-0.001A_t) & (E' \geq 5 \text{ GeV}) \end{array} \right. \\ \alpha_{2n} = \left\{ \begin{array}{ll} (0.1+0.01E')\ (1-0.001A_t) & (E' < 5 \text{ GeV}) \\ 0.15(1-0.001A_t) & (E' \geq 5 \text{ GeV}) \end{array} \right. \end{array} \right\} \tag{3.5.21}$$

The third term in the summation is the balance of cascade particles after inclusion of the quasi-elastic contribution.

The quasi-elastic contribution is estimated and includes the nuclear attenuation following the quasi-elastic event. The proton quasi-elastic cross section is

$$\begin{aligned} \sigma_{Q,pp} &= Z_t\sigma_{pp} + (A_t - Z_t)\sigma_{np} \\ \sigma_{Q,pn} &= (A_t - Z_t)\sigma_{np} \end{aligned} \tag{3.5.22}$$

and similarly for neutrons

$$\begin{aligned} \sigma_{Q,nn} &= (A_t - Z_t)\sigma_{nn} + Z_t\sigma_{np} \\ \sigma_{Q,np} &= Z_t\sigma_{np} \end{aligned} \tag{3.5.23}$$

The corresponding multiplicities are taken as

$$N_{Q,jk} = e^{-.05\sqrt{A_t}}\sigma_{Q,jk} \Big/ \sum_{\ell} \sigma_{Q,j\ell} \tag{3.5.24}$$

where the exponential factor accounts for the attenuation of the quasi-elastic particles before they escape the nucleus. The balance of the cascade particles are contained in N_3 as

$$N_3 = N_c - N_2 - N_Q \tag{3.5.25}$$

with an assumed spectral coefficient given by

$$\alpha_3 = \alpha_2/0.7 \tag{3.5.26}$$

Results of the present formalism are shown in figures 11 to 24 in comparison with the calculations of Bertini. Some further improvements in this parameterization need to be made.

3.5.4. Light fragment spectrum. The light fragment yields per event are given in table 3.5.3 as obtained from Bertini's MECC7 calculations. These results are extrapolated and interpolated in energy and mass number. The corresponding mean energies are given in table 3.5.4. The mean energies are used in Ranft's formula for nucleons and similarly for the light ions.

3.5.5. Heavy fragment spectrum. The differential spectrum of the target fragments is obtained from the momentum distributions of projectile fragments produced in collision with hydrogen targets. The fragment densities in phase space were measured by the Heckman group (ref. 35) at Lawrence Berkeley Laboratory (LBL), from which the differential energy spectrum is found to be

$$\frac{d\sigma}{dE} = \frac{\sigma_0 \exp(-E/2E_0)\sqrt{E}}{\sqrt{2\pi E_0^3}} \tag{3.5.27}$$

which is normalized such that

$$\sigma_0 = \int_0^\infty \frac{d\sigma}{dE}\, dE \tag{3.5.28}$$

is the fragmentation cross section. The value of E_0 depends on the initial target mass and the fragment mass as

$$E_0 = \Delta_p^2/2A_f \tag{3.5.29}$$

$$b = \min\left\{112A_t^{1/2}, 260\right\} \tag{3.5.30}$$

$$\delta_A = \left\{ \begin{matrix} 0.45 & (A_t = A_f) \\ A_t - A_f & (\text{Otherwise}) \end{matrix} \right\} \tag{3.5.31}$$

$$\Delta_p = 0.8b\left[\frac{4\delta A}{20(A_t - 1)}\right]^{1/2} (\text{MeV}/c) \tag{3.5.32}$$

Values of Δ_p obtained from the above are compared with experiments and results of others (ref. 35) in table 3.5.5.

In relating the ultimate effects of the interaction of nucleons in materials, the energy given over to various ion fragment types per collision event is of utmost importance. The fragmentation and energy transfer cross sections of Bertini and the present calculation are compared with the experiments of Greiner et al. in table 3.5.6. The energy transfer of the

Bertini data set is nearly half of that observed in experiments. The present result with the Rudstam cross sections is low by less than 20 percent. An ad hoc correction factor is applied to the Rudstam cross sections as shown in table 3.5.6 to better match the experimental data. Note, the corrections make the results slightly conservative.

4. Results

In an effort to begin validation of the present code, we compare the results with prior calculations using Monte Carlo methods and essentially the same data base. Fully three-dimensional Monte Carlo calculations have been made with the Bertini code as the nuclear cross section set and low energy neutron data. (See refs. 36 and 37 for a detailed discussion.) Energy absorption in a tissue slab for normally incident neutrons of energies 0.5, 2, and 10 MeV is shown in table 4.1. Also shown are the results of the present code. The results appear remarkably good considering the crudeness of the straight ahead approximation for low energy neutrons and the limitations of the present data base. Results for higher energy neutrons are shown in figures 25 to 29. In each case, reasonable agreement with the results of Zerby and Kinney is obtained. Similar results are found for energetic protons as shown in figures 30 to 33. In the present calculation, the first generation proton spectrum is discontinuous for monoenergetic beams and is best handled by taking many energy points in the spectrum. However, the calculation time then becomes excessive. The present results were calculated using only 30 energy points; this is adequate for space radiation, as shown in reference 38, but marginal for the present monoenergetic results. The use of numerical benchmark problems will allow us to better understand the numerical procedures. Such a benchmark has already provided some insight (ref. 38).

5. Concluding Remarks

The emphasis of the present report is on high energy baryon transport and a relatively complete model is presented. But it is especially important that any such code adequately represent the low energy neutrons in a reasonable way. It is seen from these results that this has been accomplished in the present code employing the straight ahead approximation. The calculated doses of 100 to 400 MeV neutrons and protons on tissue are in reasonable agreement with the more complete Monte Carlo code. The primary advantage of the present code is computer efficiency while maintaining adequate accuracy. Future work will concentrate on improving the data base to further improve the comparisons.

NASA Langley Research Center
Hampton, VA 23665-5225
May 6, 1988

6. References

1. Wilson, John W.; and Lamkin, Stanley L.: Perturbation Theory for Charged-Particle Transport in One Dimension. *Nucl. Sci. & Eng.*, vol. 57, no. 4, Aug. 1975, pp. 292–299.
2. Wilson, John W.: *Analysis of the Theory of High-Energy Ion Transport.* NASA TN D-8381, 1977.
3. Wilson, John W.; and Badavi, F. F.: Methods of Galactic Heavy Ion Transport. *Radiat. Res.*, vol. 108, 1986, pp. 231–237.
4. Wilson, J. W.; Townsend, L. W.; and Badavi, F. F.: Galactic HZE Propagation Through the Earth's Atmosphere. *Radiat. Res.*, vol. 109, no. 2, Feb. 1987, pp. 173–183.
5. Alsmiller, R. G., Jr.: High-Energy Nucleon Transport and Space Vehicle Shielding. *Nucl. Sci. & Eng.*, vol. 27, no. 2, Feb. 1967, pp. 158–189.
6. Walske, M. C.; and Bethe, H. A.: Asymptotic Formula for Stopping Power of K-Electrons. *Phys. Review*, vol. 83, 1951, pp. 457–458.
7. Bragg, W. H.; and Kleeman, R.: On the α Particles of Radium, and Their Loss of Range in Passing Through Various Atoms and Molecules. *Philos. Mag. & J. Sci.*, ser. 6, vol. 10, no. 57, Sept. 1905, pp. 318–340.

8. Platzman, Robert L.: On the Primary Processes in Radiation Chemistry and Biology. *Symposium on Radiobiology—The Basic Aspects of Radiation Effects on Living Systems*, James J. Nickson, ed., John Wiley & Sons, Inc., c.1952, pp. 97–116.
9. Wilson, J. W.; and Kamaratos, E.: Mean Excitation Energy for Molecules of Hydrogen and Carbon. *Phys. Lett.*, vol. 85A, no. 1, Sept. 7, 1981, pp. 27–29.
10. Wilson, J. W.; Chang, C. K.; Xu, Y. J.; and Kamaratos, E.: Ionic Bond Effects on the Mean Excitation Energy for Stopping Power. *J. Appl. Phys.*, vol. 53, no. 2, Feb. 1982, pp. 828–830.
11. Wilson, J. W.; and Xu, Y. J.: Metallic Bond Effects on Mean Excitation Energies for Stopping Power. *Phys. Lett.*, vol. 90A, no. 5, July 12, 1982, pp. 253–255.
12. Chu, W. K.; Moruzzi, V. L.; and Ziegler, J. F.: Calculations of the Energy Loss of ^{4}He Ions in Solid Elements. *J. Appl. Phys.*, vol. 46, no. 7, July 1975, pp. 2817–2820.
13. Andersen, H. H.; and Ziegler, J. F.: *Hydrogen Stopping Powers and Ranges in All Elements.* Pergamon Press, Inc., c.1977.
14. Janni, Joseph F.: *Calculations of Energy Loss, Range, Pathlength, Straggling, Multiple Scattering, and the Probability of Inelastic Nuclear Collisions for 0.1- to 1000-MeV Protons.* AFWL-TR-65-150, U.S. Air Force, Sept. 1966. (Available from DTIC as AD 643 837.)
15. Bichsel, Hans: Passage of Charged Particles Through Matter. *American Institute of Physics Handbook*, Second ed., Dwight E. Gray, ed., McGraw-Hill Book Co., Inc., 1963, pp. 8-20–8-47.
16. Ziegler, J. F.: *Helium Stopping Powers and Ranges in All Elemental Matter.* Pergamon Press, c.1977.
17. Barkas, Walter H.: *Nuclear Research Emulsions—I. Techniques and Theory.* Academic Press, Inc., 1963.
18. Lindhard, J.; Scharff, M.; and Schiott, H. E.: Range Concepts and Heavy Ion Ranges (Notes on Atomic Collisions, II). *Mat.-Fys. Medd. -K. Dan. Vid. Selske*, vol. 33, no. 14, 1963, pp. 1–42.
19. Matteson, S.; Powers, D.; and Chau, E. K. L.: Physical-State Effect in the Stopping Cross Section of H_2O Ice and Vapor for 0.3 to 2.0 MeV α Particles. *Phys. Review*, ser. A, vol. 15, no. 3, Mar. 1977, pp. 856–864.
20. Palmer, Rita B. J.; and Akhavan-Rezayat, Ahmad: Range-Energy Relations and Stopping Power of Water, Water Vapour and Tissue Equivalent Liquid for α Particles Over the Energy Range 0.5 to 8 MeV. *Sixth Symposium on Microdosimetry—Volume II*, J. Booz and H. G. Ebert, eds., Hardwood Academic Publ., Ltd. (London), c.1978, pp. 739–748.
21. Northcliffe, L. C.; and Schilling, R. F.: Range and Stopping-Power Tables for Heavy Ions. *Nucl. Data*, Sect. A, vol. 7, no. 3-4, Jan. 1970, pp. 233–463.
22. Fleischer, Robert L.; Price, P. Buford; and Walker, Robert M.: *Nuclear Tracks in Solids—Principles and Applications.* Univ. of California Press, c.1975.
23. Letaw, John; Tsao, C. H.; and Silberberg, R.: Matrix Methods of Cosmic Ray Propagation. *Composition and Origin of Cosmic Rays*, Maurice M. Shapiro, ed., D. Reidel Publ. Co., c.1983, pp. 337–342.
24. Hughes, Donald J.; and Schwartz, Robert B.: *Neutron Cross Sections.* BNL 325, Second ed., Brookhaven National Lab., July 1, 1958.
25. Rudstam, G.: Systematics of Spallation Yields. *Zeitschrift fur Naturforschung*, vol. 21a, no. 7, July 1966, pp. 1027–1041.
26. Silberberg, R.; Tsao, C. H.; and Letaw, John R.: Improvement of Calculations of Cross Sections and Cosmic-Ray Propagation. *Composition and Origin of Cosmic Rays*, Maurice M. Shapiro, ed., D. Reidel Publ. Co., c.1983, pp. 321–336.
27. Hellwege, K.-H., ed.: *Landolt-Börnstein Numerical Data and Functional Relationships in Science and Technology—Group I: Nuclear and Particle Physics, Volume 7, Elastic and Charge Exchange Scattering of Elementary Particles.* Springer-Verlag, 1973.
28. Bertini, Hugo W.; Guthrie, Miriam P.; and Culkowski, Arline H.: *Nonelastic Interactions of Nucleons and π-Mesons With Complex Nuclei at Energies Below 3 GeV.* ONRL-TM-3148, U.S. Atomic Energy Commission, Mar. 28, 1972.
29. Hess, Wilmot N.: Summary of High-Energy Nucleon-Nucleon Cross-Section Data. *Reviews Modern Phys.*, vol. 30, no. 2, pt. 1, Apr. 1958, pp. 368–401.
30. Wilson, John W.; and Costner, Christopher M.: *Nucleon and Heavy-Ion Total and Absorption Cross Section for Selected Nuclei.* NASA TN D-8107, 1975.
31. Fernbach, S.: Nuclear Radii as Determined by Scattering of Neutrons. *Reviews Modern Phys.*, vol. 30, no. 2, pt. 1, Apr. 1958, pp. 414–418.
32. Goldberg, Murrey D.; May, Victoria M.; and Stehn, John R.: *Angular Distributions in Neutron-Induced Reactions. Volume I, Z = 1 to 22.* BNL 400, Second ed., Vol. I, Sigma Center, Brookhaven National Lab., Oct. 1962.
33. Alsmiller, R. G., Jr.; Barish, J.; and Leimdorfer, M.: *Analytic Representation of Nonelastic Cross Sections and Particle-Emission Spectra From Nucleon-Nucleus Collisions in the Energy Range 25 to 400 MeV.* NASA CR-83981, 1967.

34. Ranft, J.: The FLUKA and KASPRO Hadronic Cascade Codes. *Computer Techniques in Radiation Transport and Dosimetry*, Walter R. Nelson and Theodore M. Jenkins, eds., Plenum Press, c.1980, pp. 339–371.
35. Greiner, D. E.; Lindstrom, P. J.; Heckman, H. H.; Cork, Bruce; and Bieser, F. S.: Momentum Distributions of Isotopes Produced by Fragmentation of Relativistic ^{12}C and ^{16}O Projectiles. *Phys. Review Lett.*, vol. 35, no. 3, July 21, 1975, pp. 152–155.
36. Irving, D. C.; Alsmiller, R. G., Jr.; and Moran, H. S.: *Tissue Current-to-Dose Conversion Factors for Neutrons With Energies From 0.5 to 60 MeV.* ORNL-4032, U.S. Atomic Energy Commission, 1967. (Available as NASA CR-87480.)
37. Zerby, C. D.; and Kinney, W. E.: *Calculated Tissue Current-to-Dose Conversion Factors for Nucleons Below 400 MeV.* ORNL-TM-1038 (Contract No. W-7405-eng-26), Oak Ridge National Lab., May 1965.
38. Wilson, John W.; Townsend, Lawrence W.; Ganapol, Barry D.; and Lamkin, Stanley L.: Methods for High Energy Hadronic Beam Transport. *Trans. American Nucl. Soc.*, vol. 56, June 1988, pp. 271–272.

Table 3.3.1. Simplified Total Neutron-Nucleus Cross Sections and Fitted Data at 20 MeV

	Cross section, mb, for—							
	^{6}Li	^{9}Be	^{11}B	^{16}O	^{27}Al	^{64}Cu	^{131}I	^{209}Pb
σ_{exp}	1250	1300	1490	1600	1850	2500	5000	5500
Equation (3.3.5)	1157	1409	1547	1833	2287	3279	4559	5692

Table 3.4.1. Ad Hoc Correction Factors for Rudstam's Formula

	Correction factor for—	
ΔA	^{12}C	^{16}O
1	1.3	1.5
2	0.5	1.0
3	0.3	1.0
4	0.1	1.0
5	1.0	1.5
6	0.35	0.5
7		0.5
8		0.5
9		0.5
10		1.0

Table 3.5.1. Number of Evaporation Nucleons Produced in Nuclear Collisions

[Values in parentheses are modified and used in the code]

	Number of nucleons produced at—					
	25 MeV	200 MeV	400 MeV	1000 MeV	2000 MeV	3000 MeV
$A_t = 12$:						
$p \rightarrow p$	0.51	0.54	0.50	0.72	0.75	0.84
$p \rightarrow n$	0.026	0.32	0.35	0.79	0.79	0.79
$n \rightarrow p$	0.052	0.30	0.35	0.73	0.73	0.80
$n \rightarrow n$	0.43	0.57	0.52	0.77 (0.71)	0.71 (0.71)	0.73
$A_t = 16$:						
$p \rightarrow p$	0.62	0.73	0.71	0.84	0.89	0.98 (0.93)
$p \rightarrow n$	0.07	0.36	0.441	0.11 (0.87)	0.93 (0.87)	0.82 (0.87)
$n \rightarrow p$	0.12	0.47	0.53	0.86	0.86	0.89
$n \rightarrow n$	0.55	0.60	0.59	0.79	0.79	0.81
$A_t = 27$:						
$p \rightarrow p$	0.54	0.99	1.03	1.36	1.49	1.86
$p \rightarrow n$	0.37	0.61	0.62	1.29	2.03 (1.92)	1.52 (1.92)
$n \rightarrow p$	0.14	0.78	0.82	1.29	1.60	1.74
$n \rightarrow n$	0.75	0.76	0.71	1.34	1.51	1.60
$A_t = 40$:						
$p \rightarrow p$	0.50	1.03	1.06	1.74	2.32	2.93
$p \rightarrow n$	0.53	1.12	1.24	2.63	3.36	3.64
$n \rightarrow p$	0.12	0.74	0.84	1.60	2.29	2.67
$n \rightarrow n$	0.89	1.39	1.44	2.76	3.25	3.54
$A_t = 65$:						
$p \rightarrow p$	0.18	0.75	0.91	2.11	3.15	4.00
$p \rightarrow n$	1.04	2.33	2.65	3.97	4.79	5.37
$n \rightarrow p$	0.03	0.49	0.66	1.90	2.98	3.61
$n \rightarrow n$	1.46	2.77	2.90	4.17	4.99	5.49
$A_t = 80$:						
$p \rightarrow p$	0.10	0.60	1.07	2.2	3.18	4.89
$p \rightarrow n$	1.29	2.20	3.18	3.72	5.07	6.77
$n \rightarrow p$	0.02	0.53	0.79	1.87	2.91	0.53
$n \rightarrow n$	1.58	3.19	3.43	4.07	5.35	6.91
$A_t = 100$:						
$p \rightarrow p$	0.03	0.46	1.28	2.96	4.56	5.78
$p \rightarrow n$	1.53	1.97	3.72	5.46	7.04	8.17
$n \rightarrow p$	0.004	0.59	0.96	2.71	4.27	5.44
$n \rightarrow n$	1.67	3.60	3.97	5.63	7.31	8.33
$A_t = 132$:						
$p \rightarrow p$	0.01	0.61	1.03	2.68	4.51	6.32
$p \rightarrow n$	1.91	4.11	5.25	8.76	11.34	12.31
$n \rightarrow p$	0.001	0.47	0.81	2.51	4.47	5.98
$n \rightarrow n$	1.96	4.73	5.59	8.93	10.6	12.42
$A_t = 164$:						
$p \rightarrow p$	0.003	0.42	0.76	2.38	4.68	6.86
$p \rightarrow n$	2.17	5.79	7.07	12.09	15.7	16.45
$n \rightarrow p$	0.003	0.28	0.58	2.30	4.68	6.52
$n \rightarrow n$	2.26	5.96	7.07	12.3	14.6	16.51
$A_t = 207$:						
$p \rightarrow p$	0.001	0.21	0.44	2.23	5.19	7.39
$p \rightarrow n$	2.29	7.22	9.24	15.3	17.81	20.6
$n \rightarrow p$	0.00	0.10	0.30	2.10	4.88	7.05
$n \rightarrow n$	2.29	7.38	9.53	15.6	18.2	20.6

Table 3.5.2. Number of Cascade Nucleons Produced in Nuclear Collisions

	Number of nucleons produced at—					
	0.25 MeV	200 MeV	400 MeV	1000 MeV	2000 MeV	3000 MeV
$A_t = 12$:						
$p \rightarrow p$	0.58	1.43	1.63	1.95	2.15	2.48
$p \rightarrow n$	0.41	0.86	0.93	1.42	1.66	2.08
$n \rightarrow p$	0.42	0.90	0.92	1.43	1.65	1.91
$n \rightarrow n$	0.56	1.42	1.69	1.95	2.27	2.57
$A_t = 16$:						
$p \rightarrow p$	0.56	1.41	1.72	2.05	2.39	2.60
$p \rightarrow n$	0.38	0.90	0.98	1.47	1.86	2.19
$n \rightarrow p$	0.38	0.91	0.96	1.49	1.85	2.01
$n \rightarrow n$	0.54	1.43	1.70	2.05	2.52	2.70
$A_t = 27$:						
$p \rightarrow p$	0.46	1.38	1.67	2.29	2.86	3.19
$p \rightarrow n$	0.34	0.97	1.16	1.86	2.54	3.25
$n \rightarrow p$	0.32	0.93	1.01	1.69	2.28	2.71
$n \rightarrow n$	0.49	1.48	1.81	2.42	3.22	3.71
$A_t = 40$:						
$p \rightarrow p$	0.40	1.33	1.69	2.32	3.01	3.53
$p \rightarrow n$	0.30	1.04	1.24	2.46	3.52	4.48
$n \rightarrow p$	0.28	0.89	1.08	1.79	2.51	3.06
$n \rightarrow n$	0.45	1.49	1.88	2.99	4.13	4.83
$A_t = 65$:						
$p \rightarrow p$	0.30	1.21	1.69	2.35	3.16	3.87
$p \rightarrow n$	0.28	1.09	1.46	3.06	4.49	5.72
$n \rightarrow p$	0.21	0.86	1.08	1.88	2.75	3.41
$n \rightarrow n$	0.40	1.53	2.00	3.55	5.03	5.95
$A_t = 80$:						
$p \rightarrow p$	0.27	1.18	1.57	2.32	3.18	3.95
$p \rightarrow n$	0.25	1.08	1.45	3.27	4.92	6.35
$n \rightarrow p$	0.19	0.81	1.04	1.86	2.78	3.54
$n \rightarrow n$	0.36	1.51	1.98	3.78	5.40	6.64
$A_t = 100$:						
$p \rightarrow p$	0.25	1.15	1.55	2.29	3.20	4.04
$p \rightarrow n$	0.22	1.06	1.52	3.47	5.35	6.98
$n \rightarrow p$	0.17	0.78	1.08	1.84	2.44	3.67
$n \rightarrow n$	0.31	1.47	2.03	3.96	5.76	7.33
$A_t = 132$:						
$p \rightarrow p$	0.20	1.00	1.46	2.21	3.17	3.87
$p \rightarrow n$	0.20	1.11	1.57	3.31	5.20	7.91
$n \rightarrow p$	0.13	0.70	1.00	1.79	2.69	3.52
$n \rightarrow n$	0.28	1.45	2.10	3.86	6.86	8.29
$A_t = 164$:						
$p \rightarrow p$	0.16	0.90	1.36	2.13	3.15	3.69
$p \rightarrow n$	0.18	1.11	1.60	3.16	5.06	8.86
$n \rightarrow p$	0.11	0.63	0.88	1.72	2.55	3.39
$n \rightarrow n$	0.26	1.42	2.11	3.56	7.94	9.25
$A_t = 208$:						
$p \rightarrow p$	0.14	0.82	1.27	2.05	7.74	3.51
$p \rightarrow n$	0.16	1.03	1.71	2.97	7.23	9.77
$n \rightarrow p$	0.09	0.58	0.87	1.67	2.41	3.24
$n \rightarrow n$	0.23	1.36	2.10	3.36	7.63	10.21

Table 3.5.3. Evaporated Ion Yields From Nucleon-Nucleus Collisions

[Values in parentheses are for proton reactions]

	Ion yields at—			
	500 MeV	1000 MeV	2000 MeV	3000 MeV
$A_t = 16$:				
d	0.111 (0.094)	0.199 (0.237)	0.257 (0.265)	0.304 (0.311)
t	0.022 (0.029)	0.024 (0.025)	0.033 (0.025)	0.029 (0.029)
he	0.018 (0.034)	0.035 (0.043)	0.037 (0.052)	0.037 (0.048)
α	0.664 (0.400)	0.720 (0.696)	0.664 (0.624)	0.640 (0.667)
$A_t = 27$:				
d	0.126 (0.130)	0.245 (0.269)	0.380 (0.396)	0.442 (0.433)
t	0.028 (0.023)	0.048 (0.052)	0.063 (0.065)	0.072 (0.069)
he	0.042 (0.035)	0.067 (0.074)	0.073 (0.091)	0.083 (0.092)
α	0.370 (0.400)	0.550 (0.566)	0.597 (0.582)	0.577 (0.577)
$A_t = 65$:				
d	0.150 (0.171)	0.379 (0.390)	0.748 (0.766)	0.935 (0.987)
t	0.031 (0.035)	0.075 (0.068)	0.145 (0.145)	0.177 (0.191)
he	0.013 (0.014)	0.039 (0.056)	0.112 (0.124)	0.166 (0.177)
α	0.124 (0.137)	0.231 (0.231)	0.373 (0.377)	0.431 (0.441)
$A_t = 100$:				
d	0.174 (0.183)	0.456 (0.475)	1.01 (1.02)	1.44 (1.48)
t	0.028 (0.029)	0.080 (0.081)	0.207 (0.192)	0.269 (0.273)
he	0.012 (0.017)	0.055 (0.060)	0.162 (0.185)	0.249 (0.262)
α	0.158 (0.156)	0.320 (0.339)	0.490 (0.467)	0.549 (0.540)
$A_t = 207$:				
d	0.131 (0.152)	0.536 (0.565)	1.51 (1.57)	2.54 (2.54)
t	0.038 (0.037)	0.152 (0.163)	0.415 (0.424)	0.641 (0.644)
he	0.001 (0.002)	0.017 (0.017)	0.112 (0.106)	0.211 (0.239)
α	0.053 (0.063)	0.195 (0.210)	0.527 (0.514)	0.751 (0.746)

Table 3.5.4. Mean Energies (MeV) of Light Nuclear Fragments Produced in Nucleon-Nucleus Collisions

[Values in parentheses are for proton reactions]

	Mean energies at—			
	500 MeV	1000 MeV	2000 MeV	3000 MeV
$A_t = 16$:				
n	5.55 (6.19)	7.91 (7.89)	9.55 (9.81)	11.1 (9.80)
p	6.10 (6.40)	8.33 (8.69)	9.71 (10.2)	10.3 (11.2)
d	8.53 (7.64)	12.2 (10.7)	14.9 (14.8)	16.3 (13.0)
t	6.40 (7.83)	10.6 (10.4)	12.5 (9.74)	13.7 (10.1)
he	12.1 (8.76)	11.8 (11.2)	11.1 (13.1)	12.9 (10.3)
α	9.36 (6.24)	12.6 (12.3)	13.1 (14.6)	13.6 (13.8)
$A_t = 27$:				
n	5.08 (5.09)	7.34 (7.48)	9.91 (10.5)	11.6 (12.0)
p	6.87 (6.90)	8.61 (8.92)	11.1 (11.9)	13.5 (13.7)
d	9.57 (9.42)	10.8 (11.2)	14.3 (14.8)	17.2 (17.4)
t	9.16 (9.54)	10.8 (11.1)	13.0 (13.9)	16.6 (13.7)
he	10.5 (10.8)	12.5 (12.8)	13.4 (14.1)	14.4 (14.5)
α	12.7 (13.4)	13.2 (13.6)	13.8 (13.8)	14.5 (14.6)
$A_t = 65$:				
n	4.24 (4.32)	5.67 (5.70)	7.92 (7.91)	9.67 (9.58)
p	8.25 (8.30)	9.66 (9.76)	12.1 (12.3)	14.4 (14.2)
d	9.88 (10.1)	13.5 (11.8)	13.8 (14.2)	15.6 (15.9)
t	10.0 (10.0)	11.7 (11.6)	13.7 (13.8)	15.1 (15.9)
he	14.6 (14.1)	16.4 (16.2)	17.5 (19.3)	19.5 (19.2)
α	12.7 (13.4)	13.2 (13.6)	13.8 (13.8)	14.5 (14.6)
$A_t = 100$:				
n	3.90 (3.90)	5.13 (5.16)	7.11 (7.04)	8.61 (8.74)
p	9.63 (9.62)	11.0 (11.0)	12.9 (13.2)	14.6 (14.7)
d	11.0 (11.1)	12.5 (12.6)	14.4 (15.0)	16.1 (16.0)
t	11.3 (11.7)	12.6 (13.0)	14.7 (14.3)	15.5 (16.5)
he	17.8 (18.7)	18.6 (18.8)	20.9 (20.6)	21.8 (22.2)
α	16.5 (16.5)	16.8 (16.9)	17.5 (17.5)	17.6 (17.6)
$A_t = 207$:				
n	3.28 (3.27)	4.37 (4.33)	5.83 (5.78)	6.90 (6.95)
p	12.5 (12.5)	12.2 (13.4)	14.9 (14.9)	16.2 (16.3)
d	13.2 (13.2)	14.4 (14.2)	16.0 (16.8)	17.4 (17.8)
t	13.6 (13.8)	5.0 (15.3)	16.6 (16.8)	17.4 (17.8)
he	24.1 (27.0)	26.2 (26.5)	28.0 (27.8)	29.1 (28.5)
α	25.3 (25.7)	26.0 (26.3)	26.4 (26.3)	25.9 (26.4)

Table 3.5.5. Δ_p for ^{16}O Fragments Produced by 2.1 GeV Protons

Fragment	Value of Δ_p, MeV/c, from—		
	Experiments (ref. 35)	Present work	Greiner
^{15}O	94 ± 3	80.0	83.8
^{14}O	99 ± 6	109.5	113.1
^{13}O	143 ± 14	129.2	133.5
^{16}N	54 ± 11	55.0	?
^{15}N	95 ± 3	80.0	82.8
^{14}N	112 ± 3	109.5	113.0
^{13}N	134 ± 2	129.2	133.5
^{12}N	153 ± 11	143.4	148.1
^{15}C	125 ± 19	80.0	82.8
^{14}C	125 ± 3	109.5	113.1
^{13}C	130 ± 3	129.2	133.5
^{12}C	120 ± 4	143.36	148.09
^{11}C	162 ± 5	153.45	158.5
^{10}C	190 ± 9	160.3	165.6
^{13}B	166 ± 10	129.2	133.5
^{12}B	163 ± 8	143.4	148.1
^{11}B	160 ± 2	153.5	158.5
^{10}B	175 ± 7	160.3	165.6
^{8}B	175 ± 22	165.5	171.01
^{11}Be	197 ± 20	153.5	158.5
^{10}Be	159 ± 6	160.0	165.0
^{7}Be	166 ± 2	164.24	169.66
^{9}Li	188 ± 15	164.24	169.66
^{8}Li	170 ± 13	165.4	171.0
^{7}Li	163 ± 4	164.2	169.66
^{6}He	167 ± 20	160.0	165.0

Table 3.5.6. Fragmentation Cross Sections and Fragment Energy Transfer Cross Sections From Rudstam, Bertini, and Experiments (Grainer)

[Values in parentheses include the ad hoc factor]

	Fragmentation cross sections, σ, mb, from—			Energy transfer cross sections, $\bar{E}\sigma$, MeV-mb, from—			
A_F	Bertini	Greiner	Rudstam	Bertini	Greiner	Rudstam	Ad hoc factor
16	4.69	0.02		5.04	0.0006		
15	103.4	61.5	24.8	60.6	56.9	17.0	3
14	40.0	35.4	23.6	48.8	51.7	32.3	2
13	18.5	22.8	22.4	37.6	48.3	46.0	
12	32.2	34.1	22.0	85.8	68.2	60.3	
11	8.2	26.4	17.1	37.9	99.1	58.2	1.3
10	11.0	12.7	20.6	52.8	62.0	84.6	
9	1.2	5.2	12.8	6.5	25.7	61.4	0.5
8	.56	1.23	1.87	2.5	7.1	10.4	
7	.16	27.9	9.1	6.11	153.4	56.1	3
6	5.46	17.5	18.0	31.4	92.5	123.3	
Total	225.4	244.8	172.3 (265.8)	375.1	664.9	549.6 (741)	

Table 4.1. Energy Deposition of 0.5–10 MeV Neutrons

[Values in parentheses are from present calculations]

Incident energy, MeV	Depth, cm		Energy deposition from Monte Carlo and present calculations, MeV			
			Proton		Heavy ion	
0.5	0–1	(1)	0.1107	0.0767	0.0073	0.0052
	1–2		.0986		.0066	
	4–5	(5)	.0418	(.0296)	.0028	(.0021)
	5–6		.0331		.0018	
	9–10	(10)	.0074	.0085)	.0003	(.0005)
	10–11		.0059		.0002	
	14–15	(15)	.0006	(.0016)		(.0001)
	15–16		.0007			
	19–20	(20)	.0002	(.0005)		
	20–21		.0001			
2	0–1	(1)	0.2138	(0.1773)	0.0147	(0.0124)
	1–2		.1984		.0133	
	4–5	(5)	.1539	(.1122)	.0110	(.0074)
	5–6		.1349		.0105	
	9–10	(10)	.0770	(.0602)	.0054	(.0045)
	10–11		.0741		.0061	
	14–15	(15)	.0301	(.0301)	.0026	(.0023)
	15–16		.0240		.0019	
	19–20	(20)	.0091	(.0142)	.0008	(.0011)
	20–21		.0114		.0009	
10	0–1	(1)	0.3520	(0.3056)	0.0339	(0.0376)
	1–2		.3284		.0342	
	4–5	(5)	.3220	(.2249)	.0345	(.0267)
	5–6		.2977		.0266	
	9–10	(10)	.2674	(.1537)	.0257	(.0176)
	10–11		.2661		.0225	
	14–15	(15)	.2161	(.1049)	.0203	(.0108)
	15–16		.2211		.0198	
	19–20	(20)	.1635	(.0714)	.0150	(.0078)
	20–21		.1291		.0149	

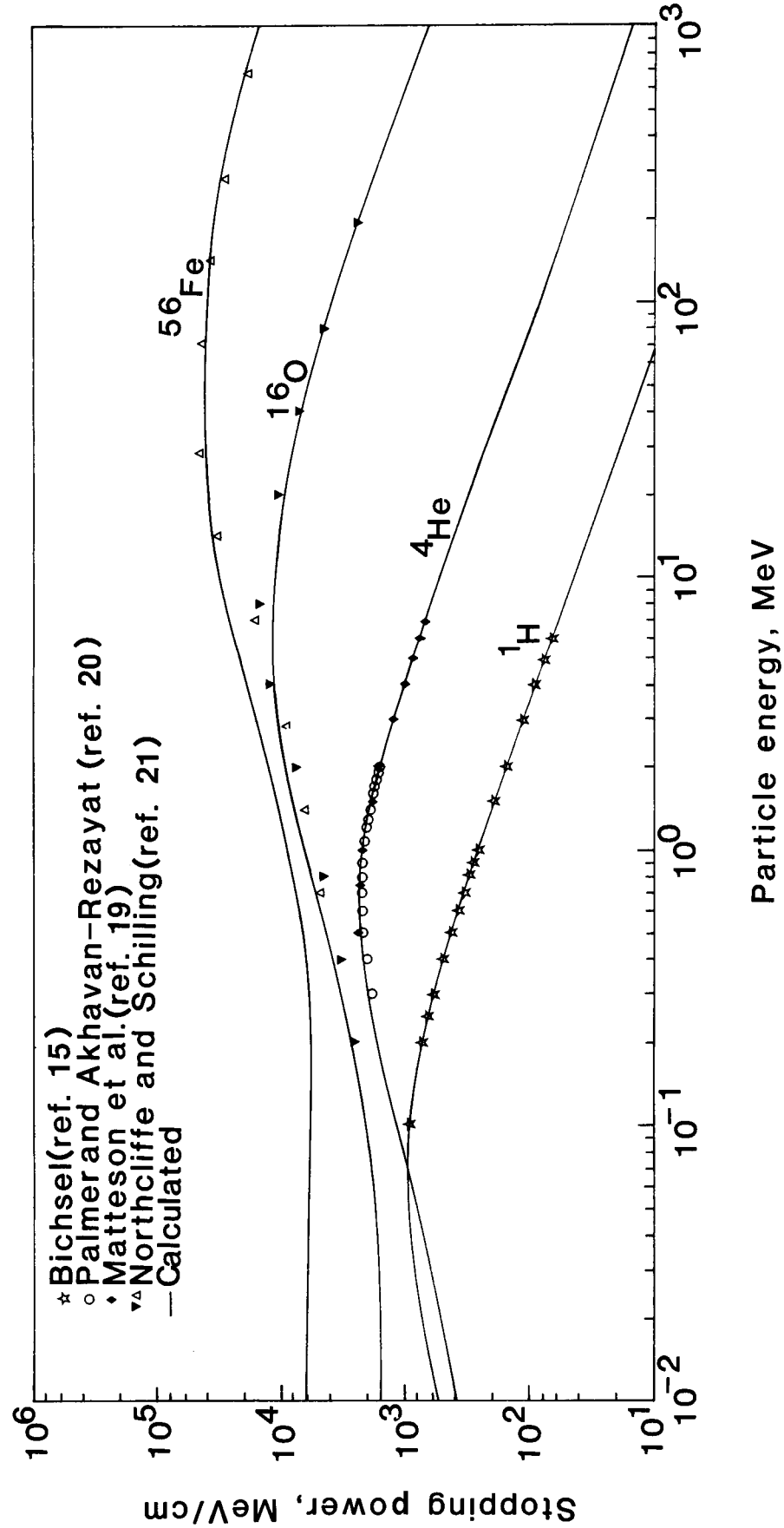

Figure 1. Calculated and experimental stopping powers in water for typical cosmic ray ions as a function of kinetic energy.

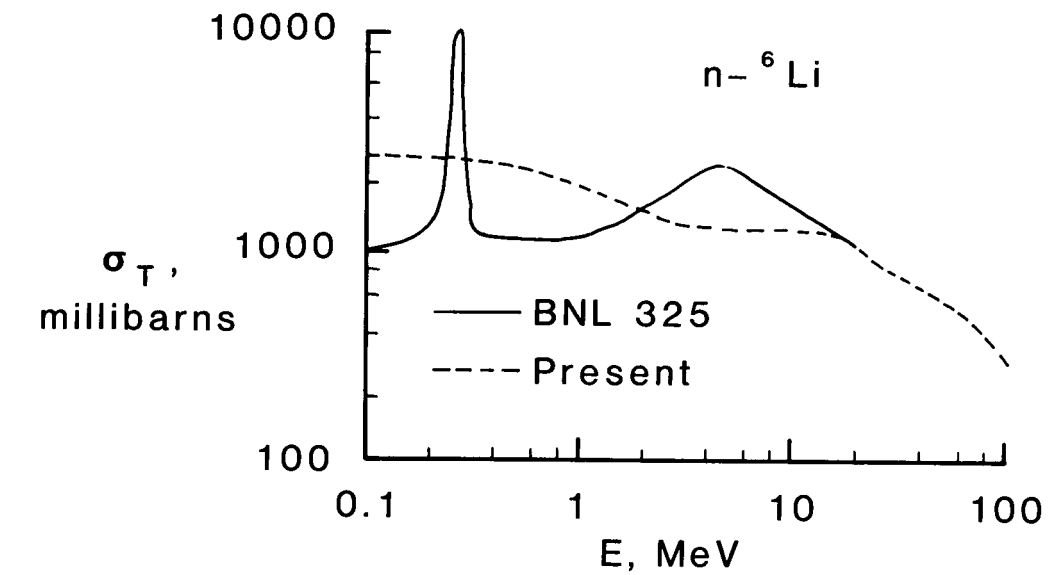

Figure 2. Total cross section of neutrons with lithium-6 as represented in the present code and according to experiment (ref. 24).

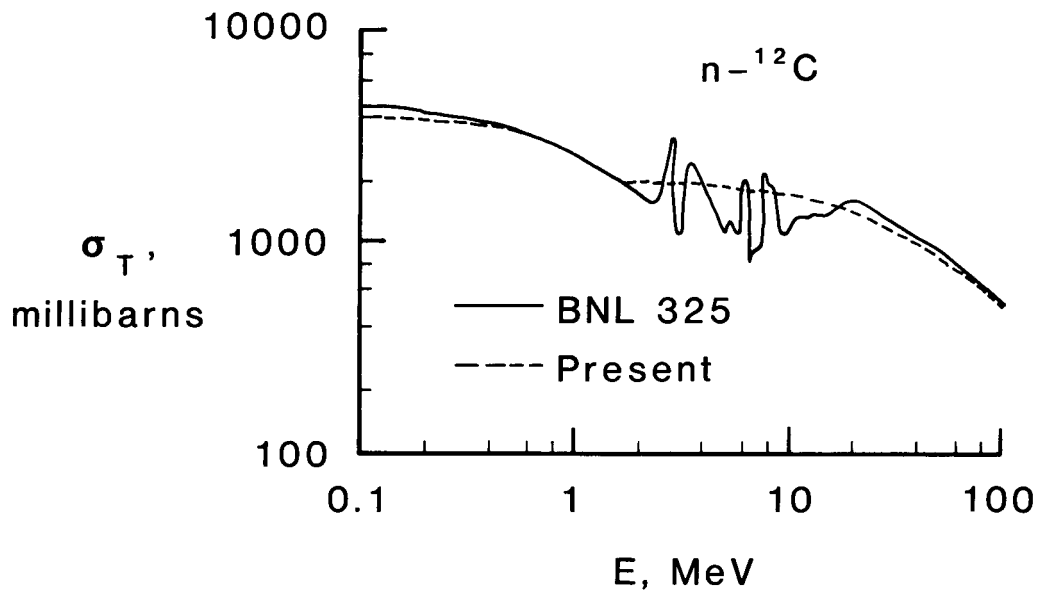

Figure 3. Total cross section for neutrons with carbon-12 according to present code and experiments (ref. 24).

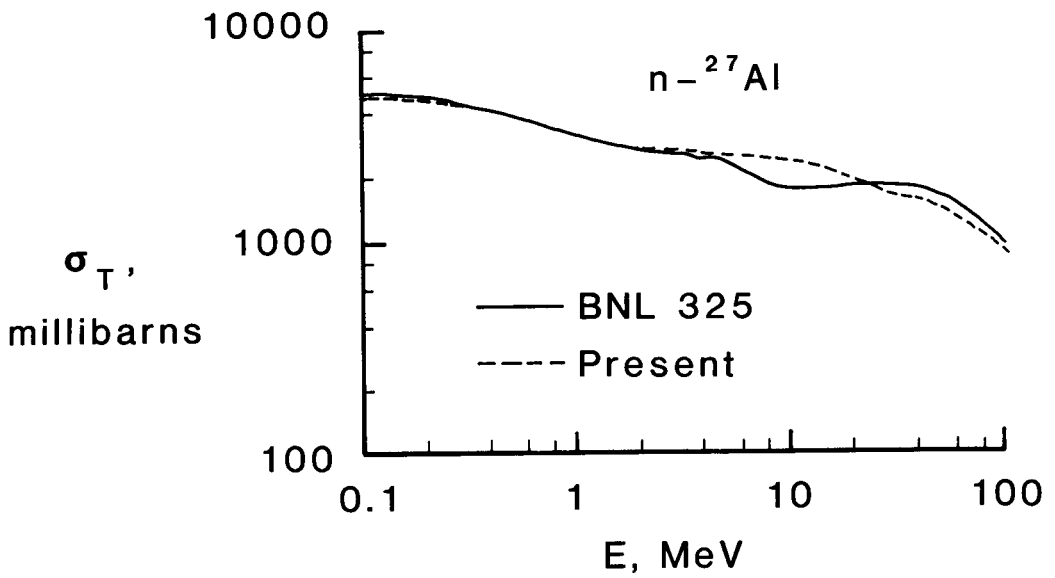

Figure 4. Total cross section for neutrons with aluminum-27 according to present code and experiments (ref. 24).

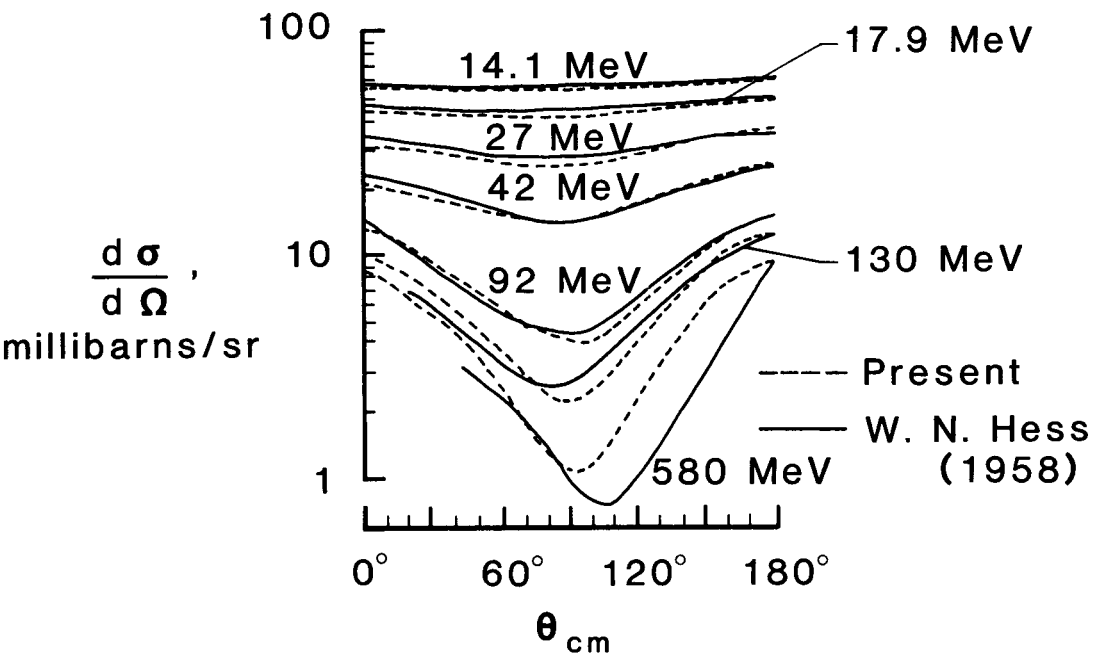

Figure 5. Neutron-proton scattering cross sections according to present code and experiment.

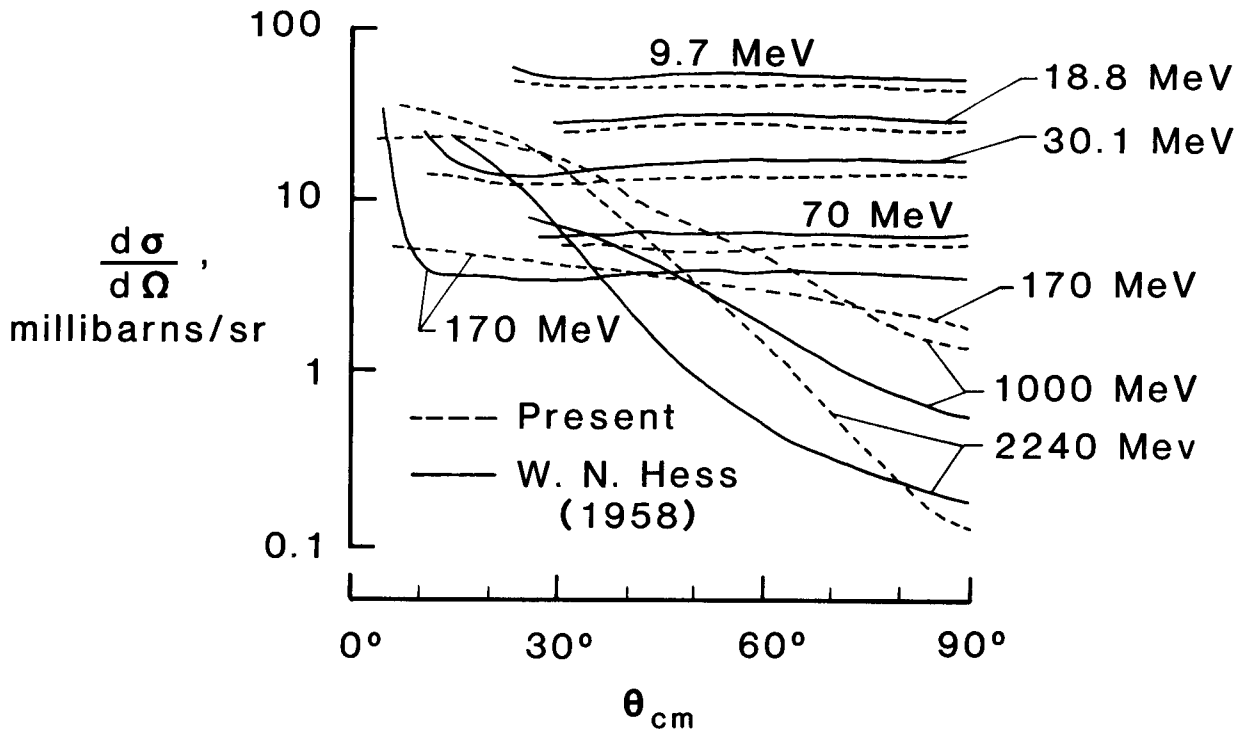

Figure 6. Proton-proton scattering cross sections according to present code and experiment.

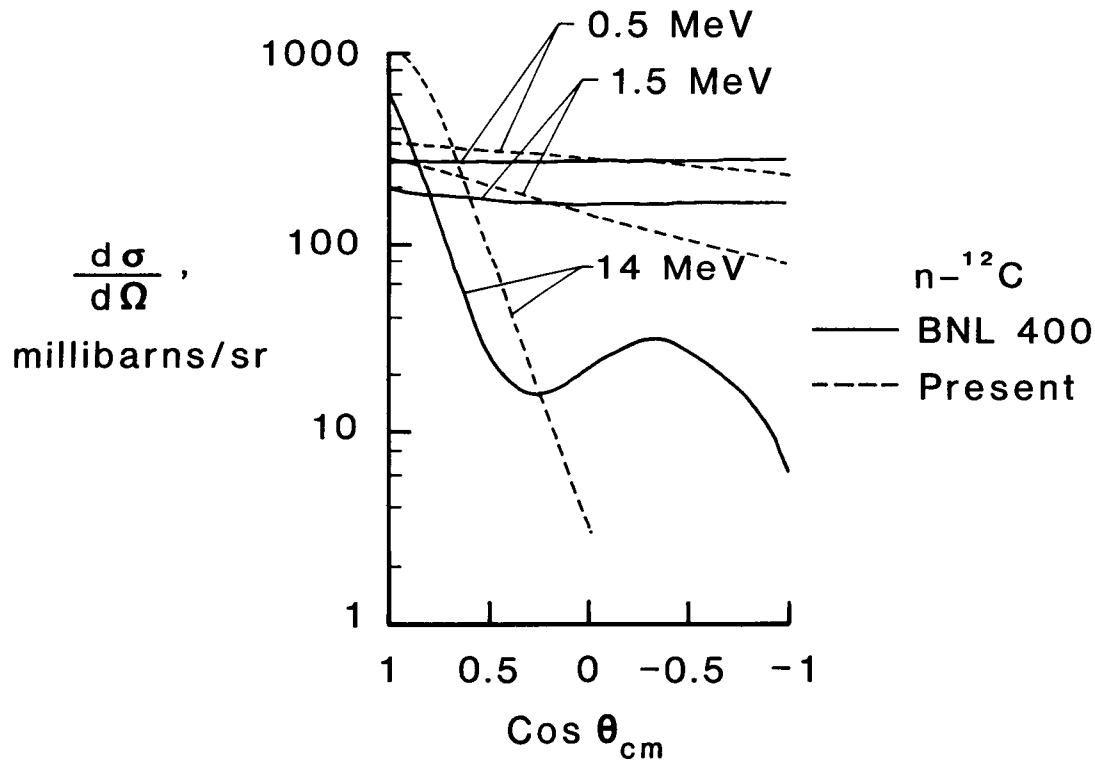

Figure 7. Neutron-carbon scattering cross sections according to present code and experiment (ref. 32).

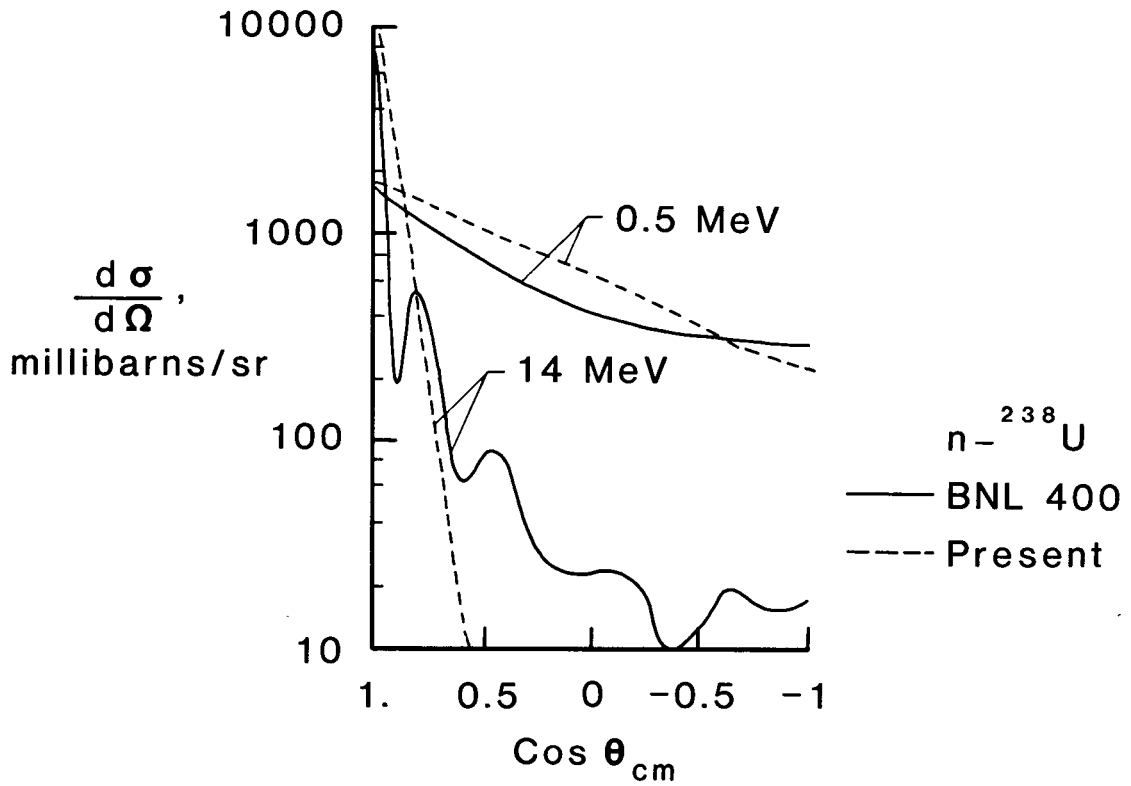

Figure 8. Neutron-uranium scattering cross sections according to present code and experiment (ref. 32).

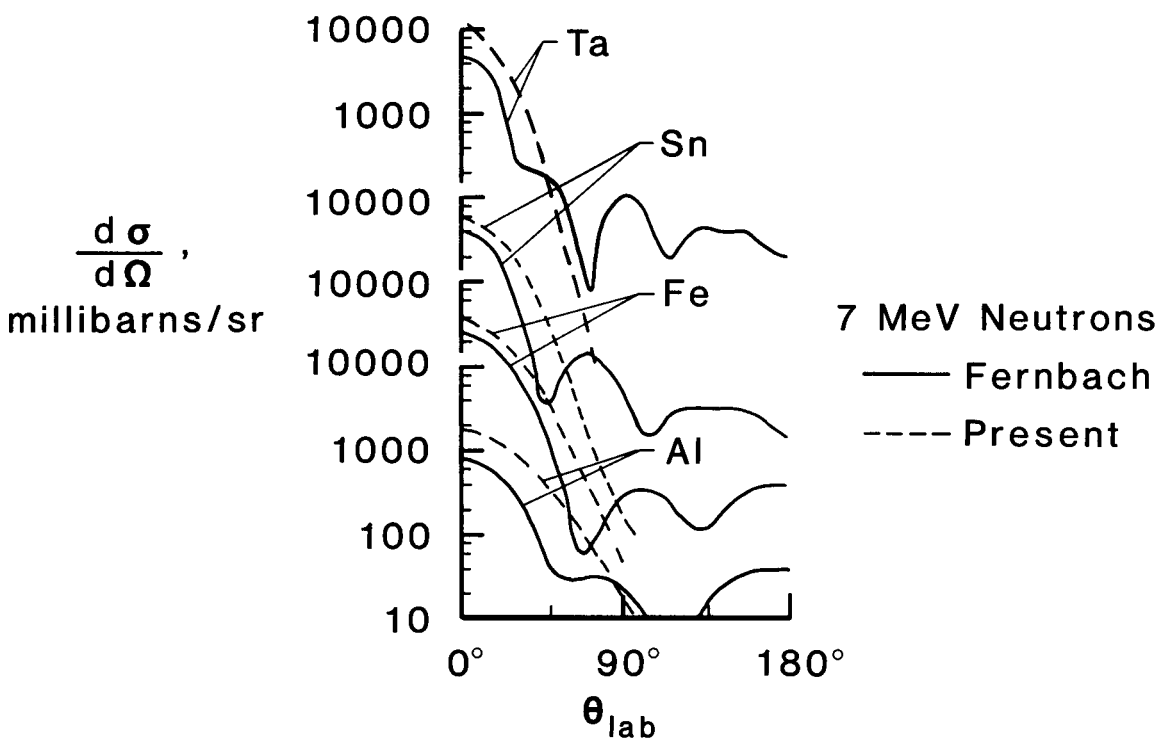

Figure 9. Neutron scattering cross sections for several elements according to present code and experiments.

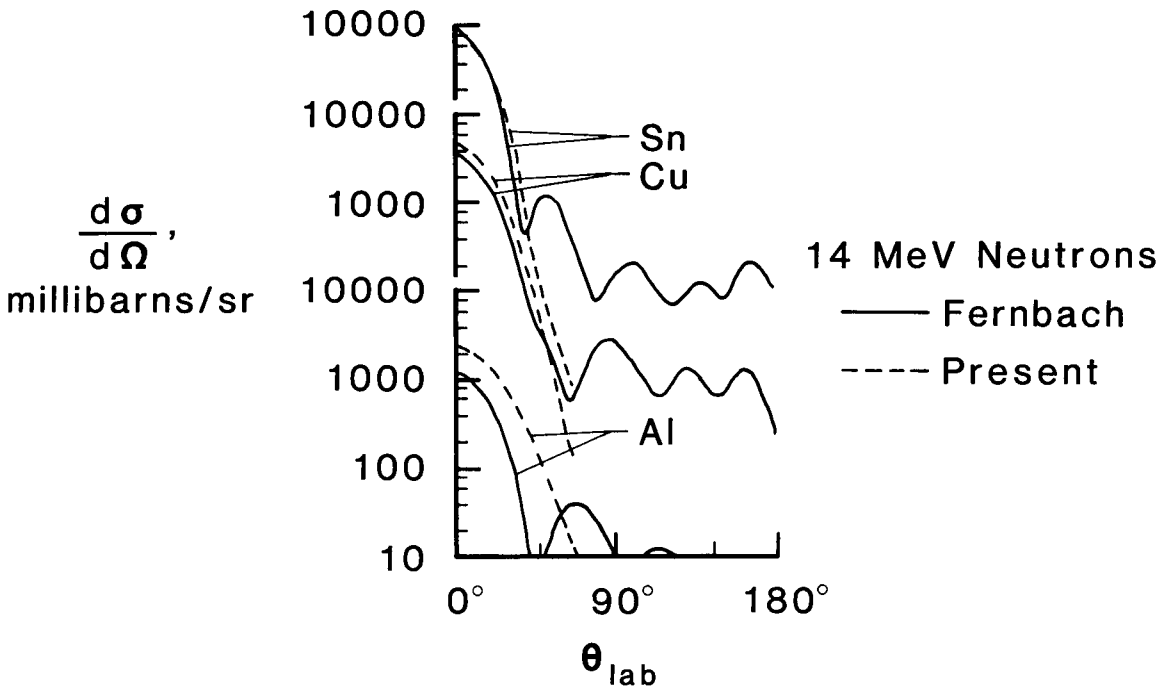

Figure 10. Neutron scattering cross sections for several elements according to present code and experiments.

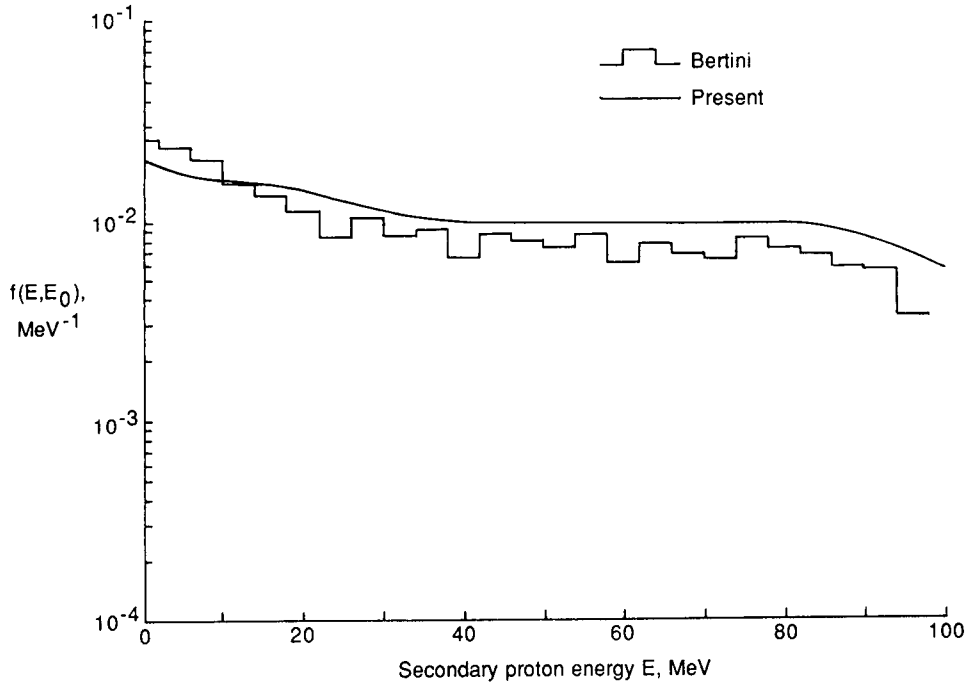

Figure 11. Nucleon cascade spectra of Bertini and the present work. Protons produced by 100 MeV protons on oxygen.

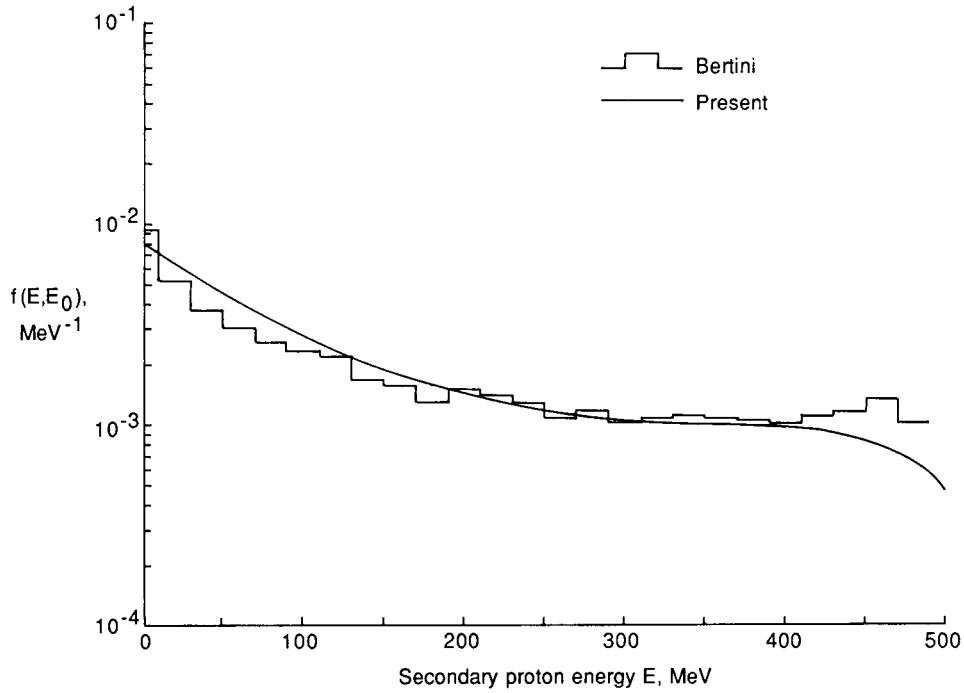

Figure 12. Nucleon cascade spectra of Bertini and the present work. Protons produced by 500 MeV protons on oxygen.

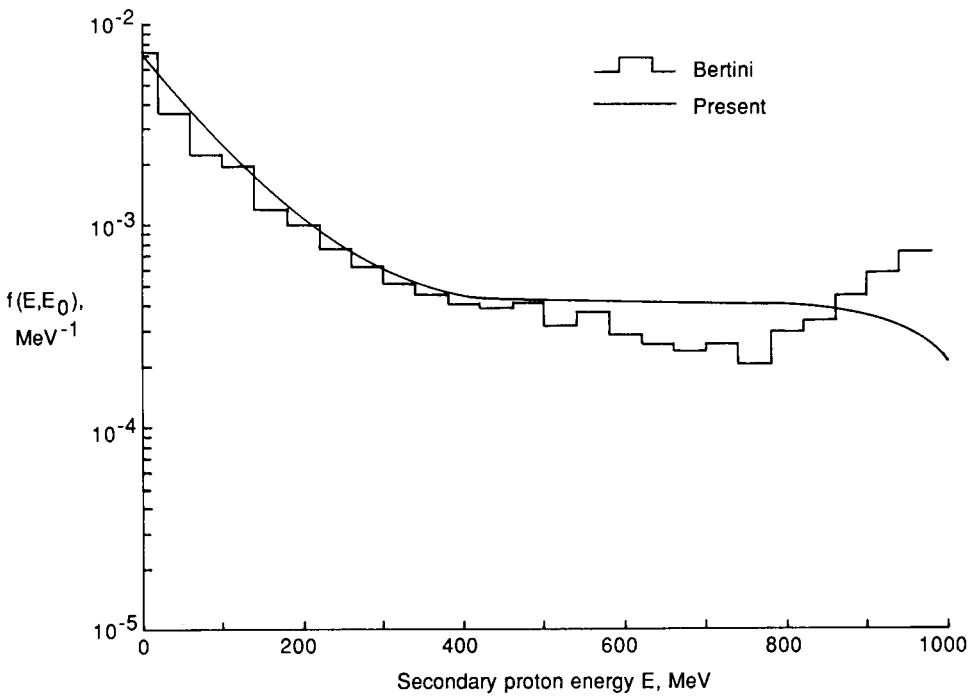

Figure 13. Nucleon cascade spectra of Bertini and the present work. Protons produced by 1000 MeV protons on oxygen.

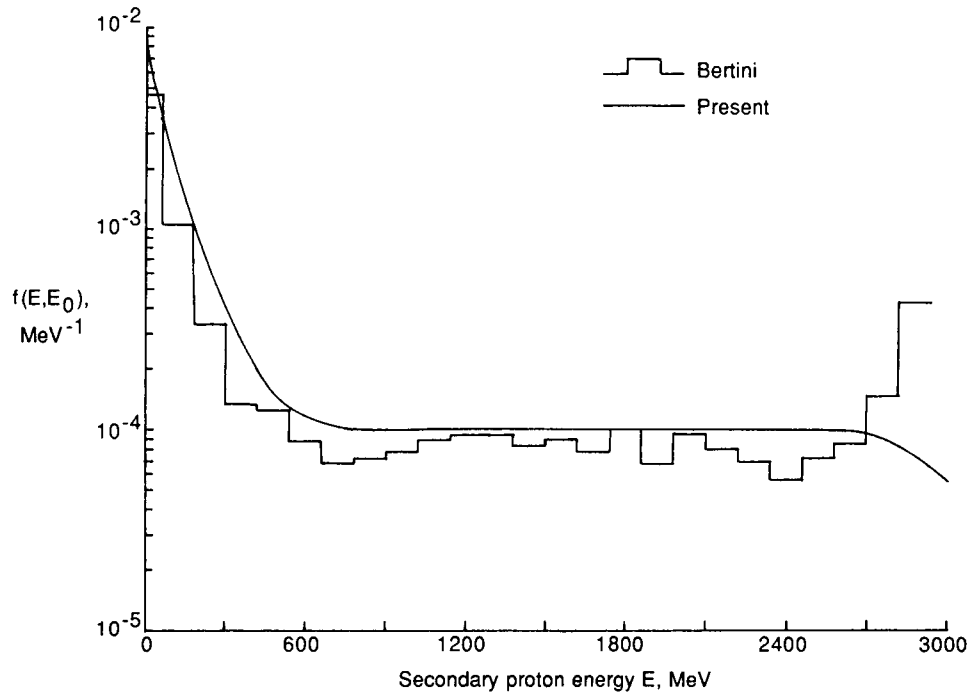

Figure 14. Nucleon cascade spectra of Bertini and the present work. Protons produced by 3000 MeV protons on oxygen.

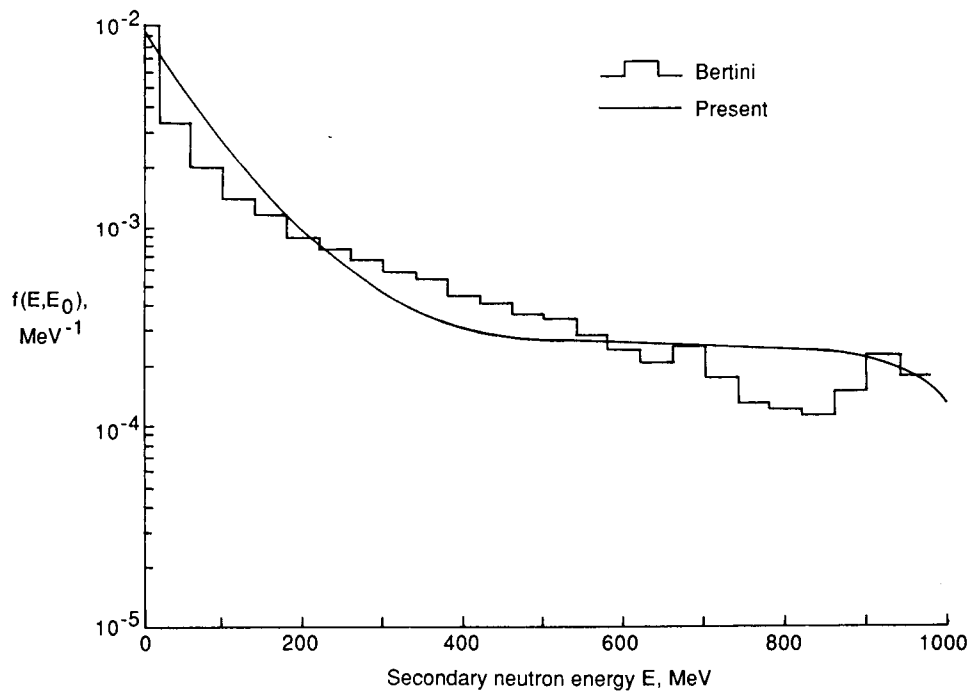

Figure 15. Nucleon cascade spectra of Bertini and the present work. Neutrons produced by 1000 MeV protons on oxygen.

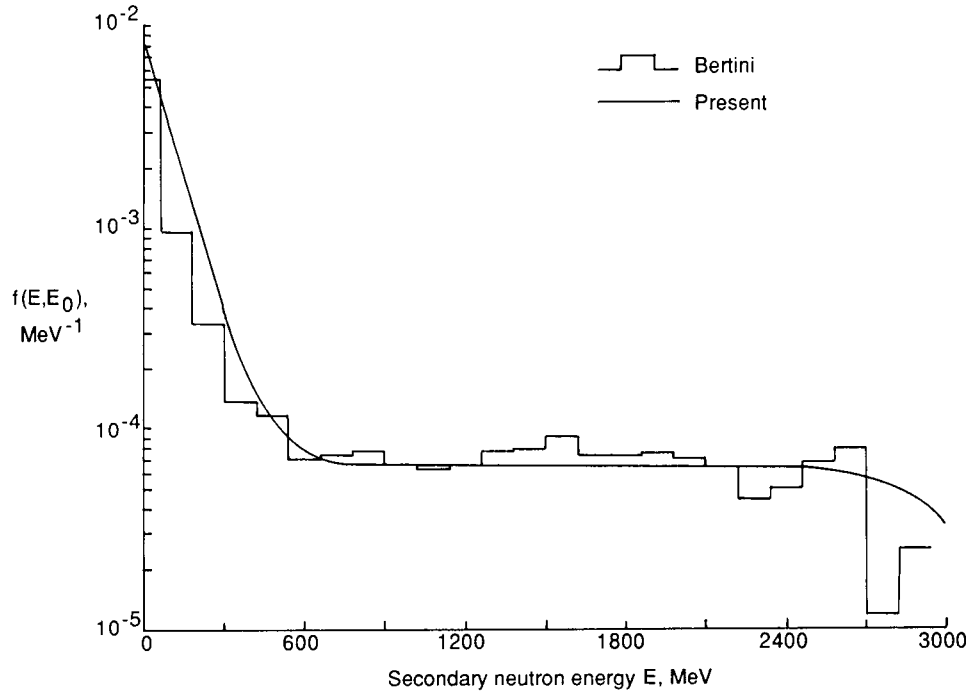

Figure 16. Nucleon cascade spectra of Bertini and the present work. Neutrons produced by 3000 MeV protons on oxygen.

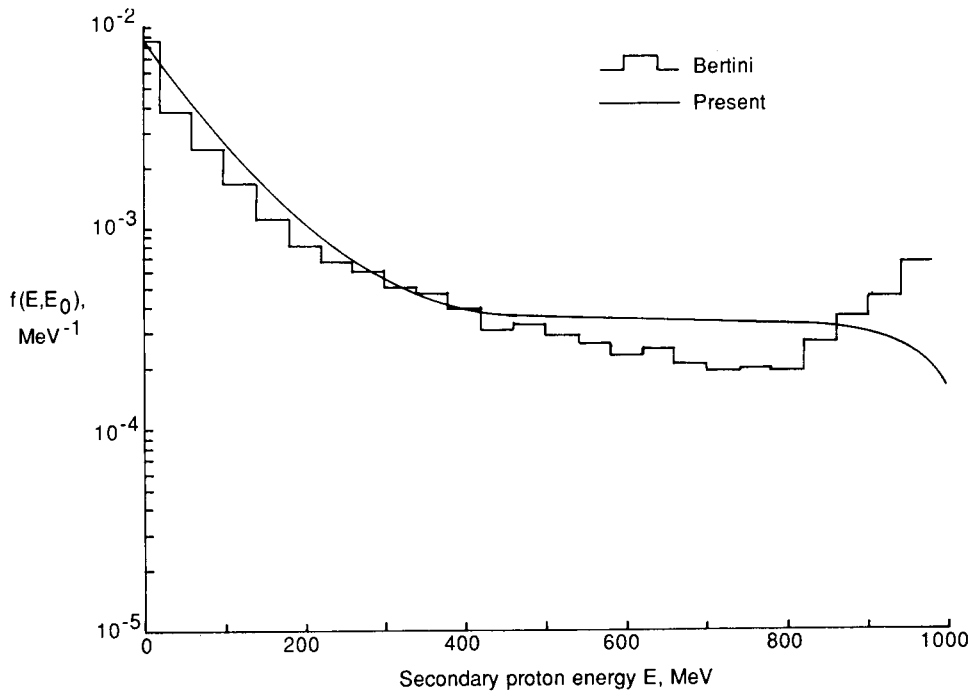

Figure 17. Nucleon cascade spectra of Bertini and the present work. Protons produced by 1000 MeV protons on aluminum.

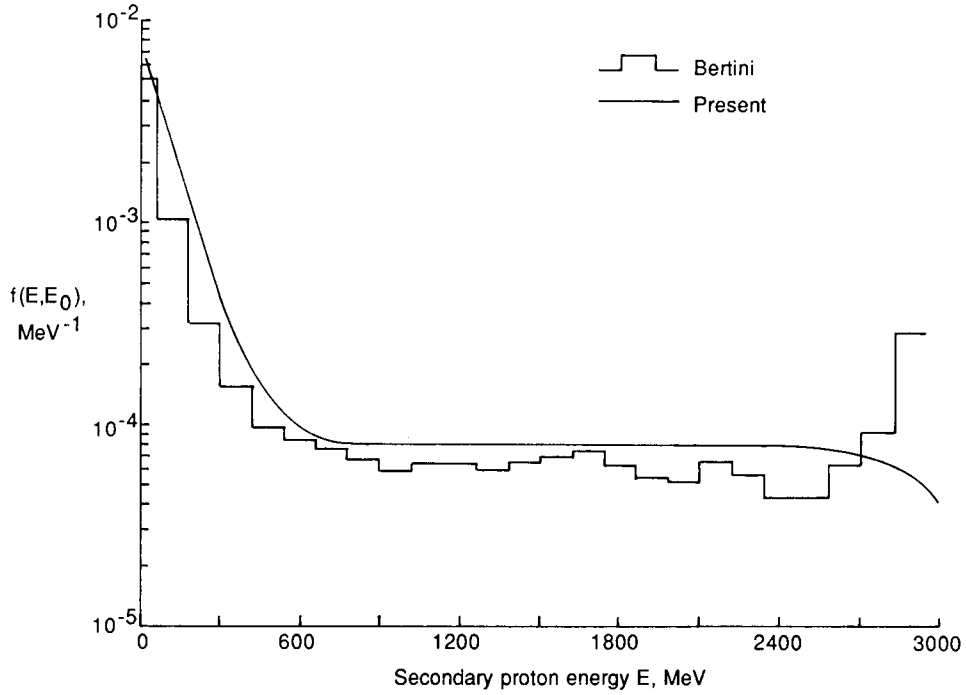

Figure 18. Nucleon cascade spectra of Bertini and the present work. Protons produced by 3000 MeV protons on aluminum.

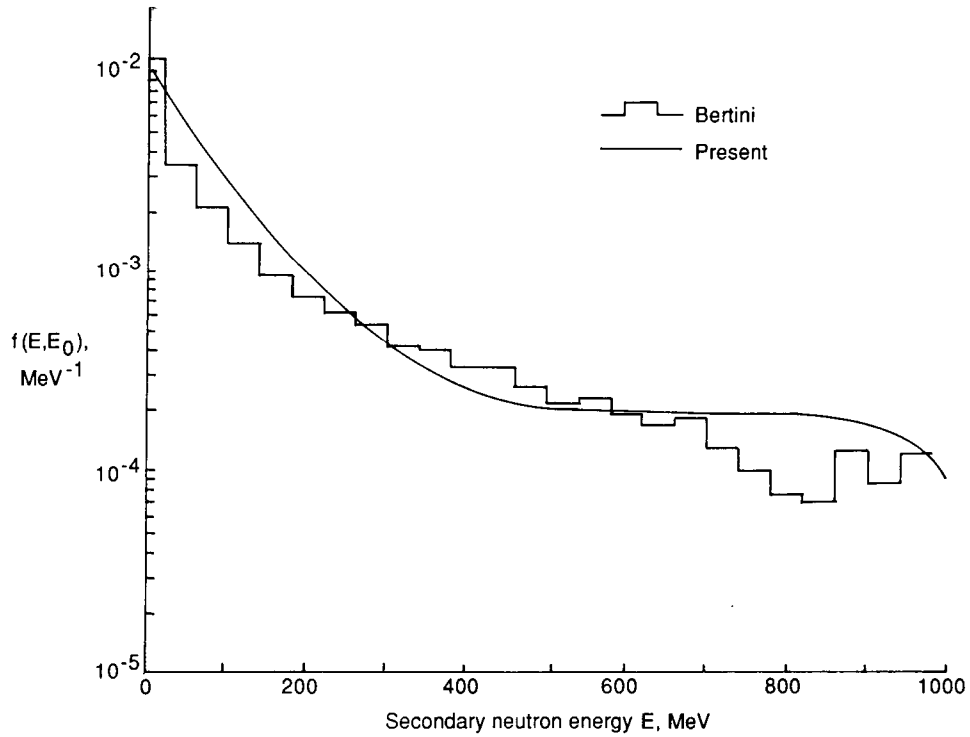

Figure 19. Nucleon cascade spectra of Bertini and the present work. Neutrons produced by 1000 MeV protons on aluminum.

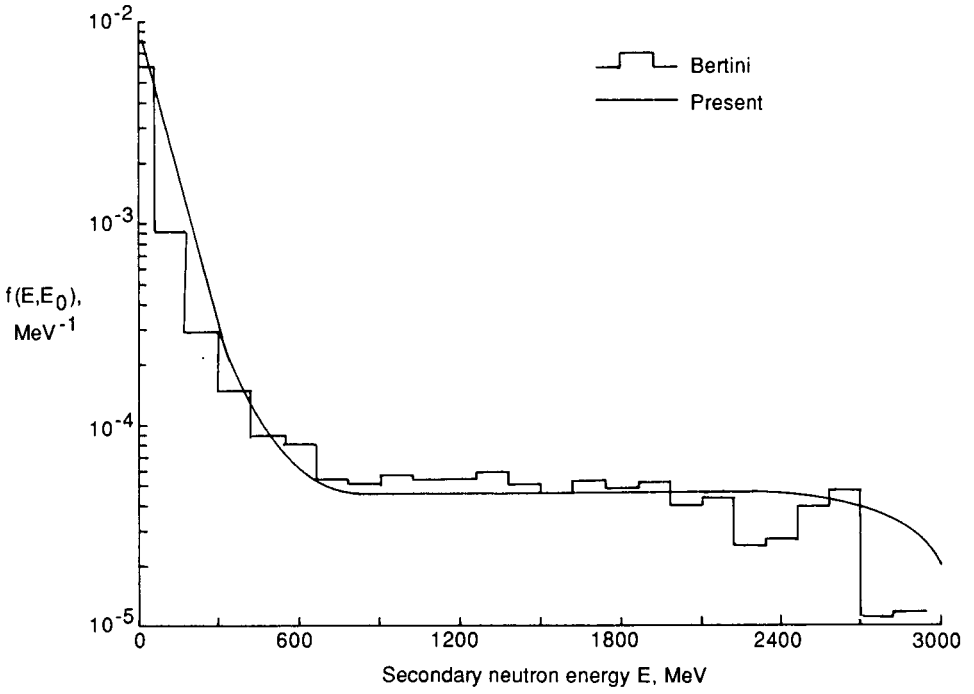

Figure 20. Nucleon cascade spectra of Bertini and the present work. Neutrons produced by 3000 MeV protons on aluminum.

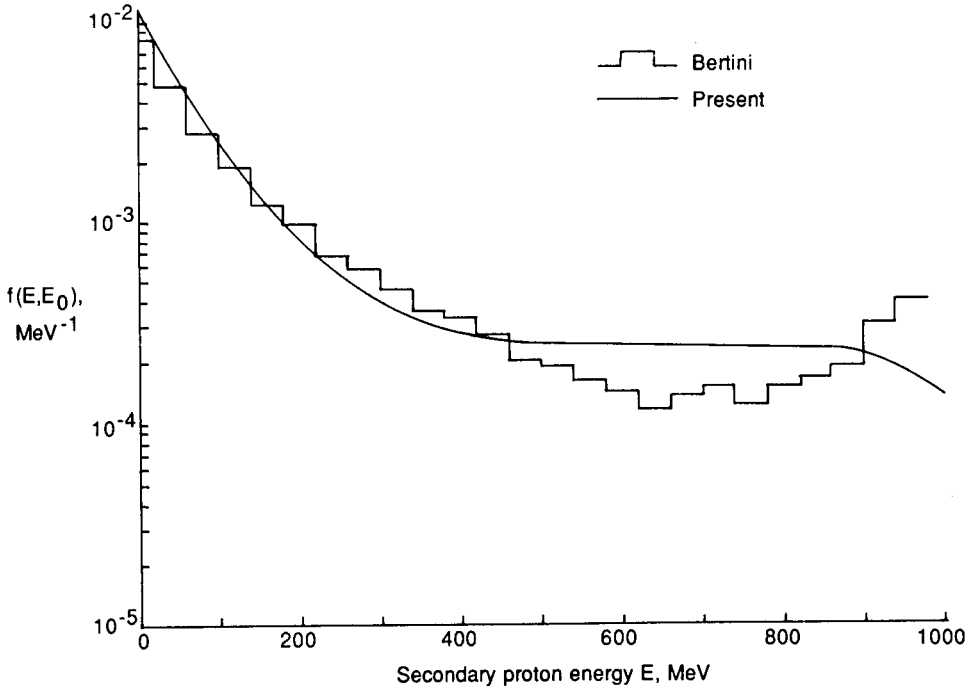

Figure 21. Nucleon cascade spectra of Bertini and the present work. Protons produced by 1000 MeV protons on lead.

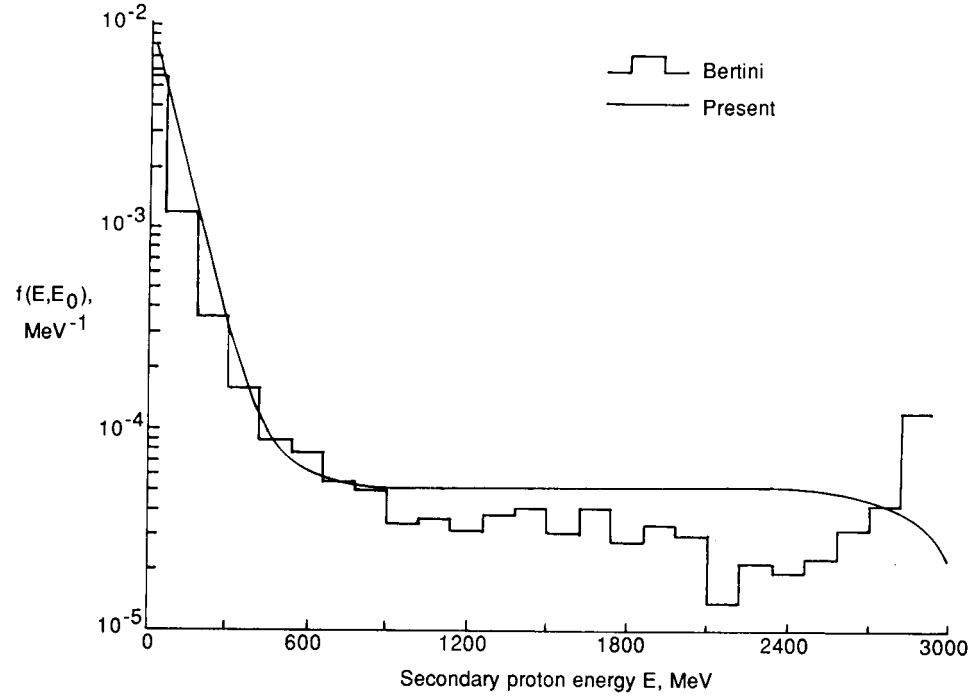

Figure 22. Nucleon cascade spectra of Bertini and the present work. Protons produced by 3000 MeV protons on lead.

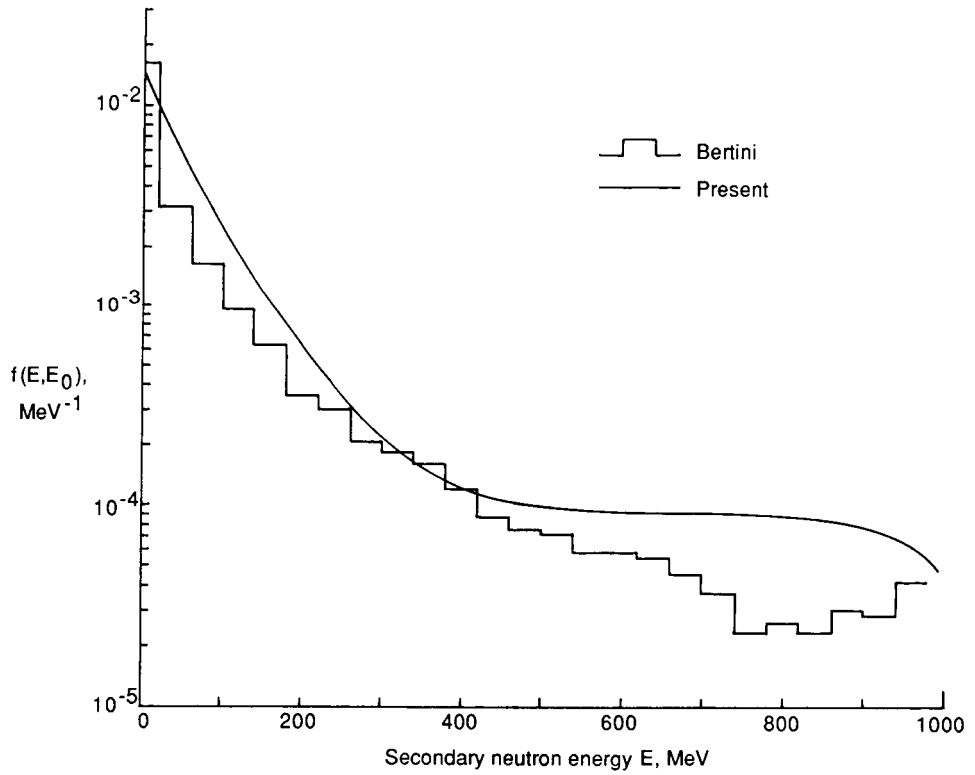

Figure 23. Nucleon cascade spectra of Bertini and the present work. Neutrons produced by 1000 MeV protons on lead.

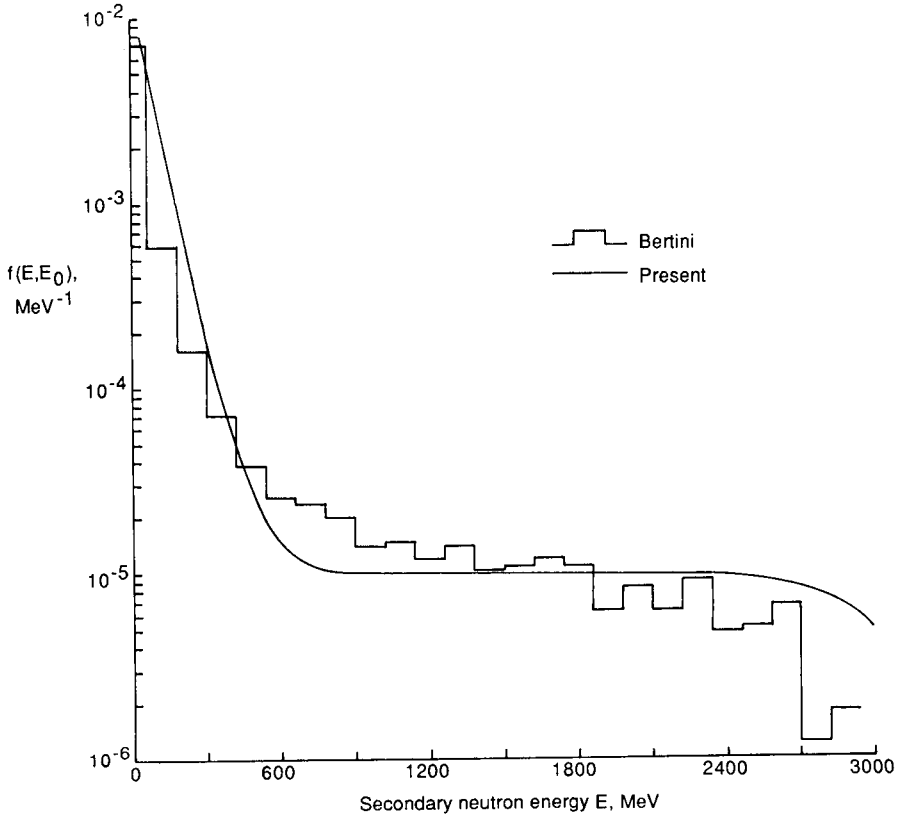

Figure 24. Nucleon cascade spectra of Bertini and the present work. Neutrons produced by 3000 MeV protons on lead.

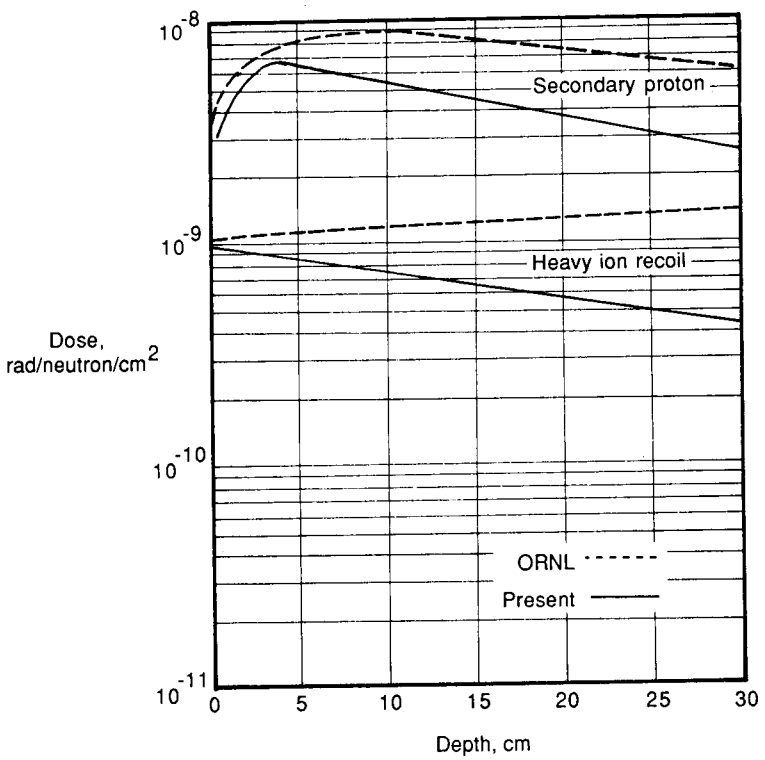

Figure 25. Dose in tissue due to normal incident 60 MeV neutrons according to reference 37 and present code.

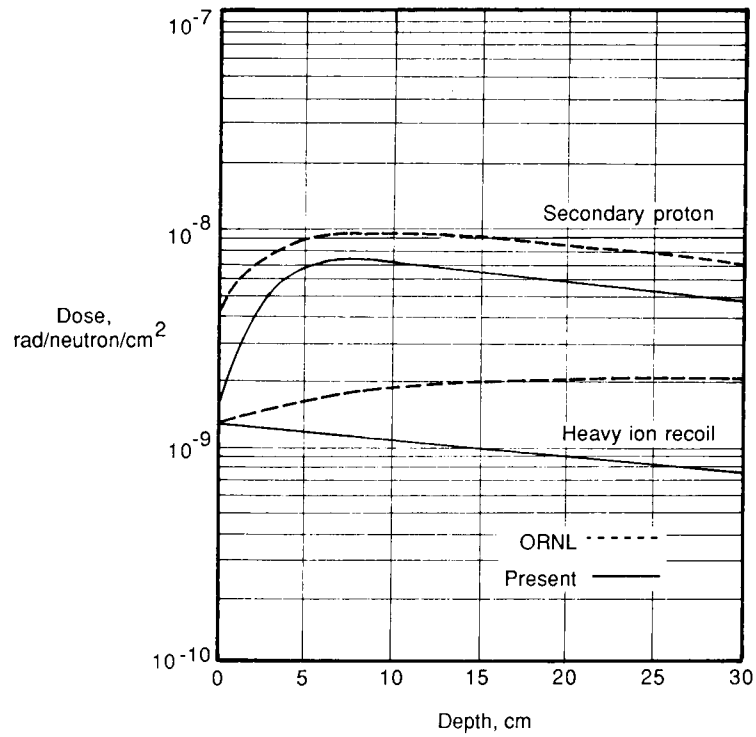

Figure 26. Dose in tissue due to normal incident 100 MeV neutrons according to reference 37 and present code.

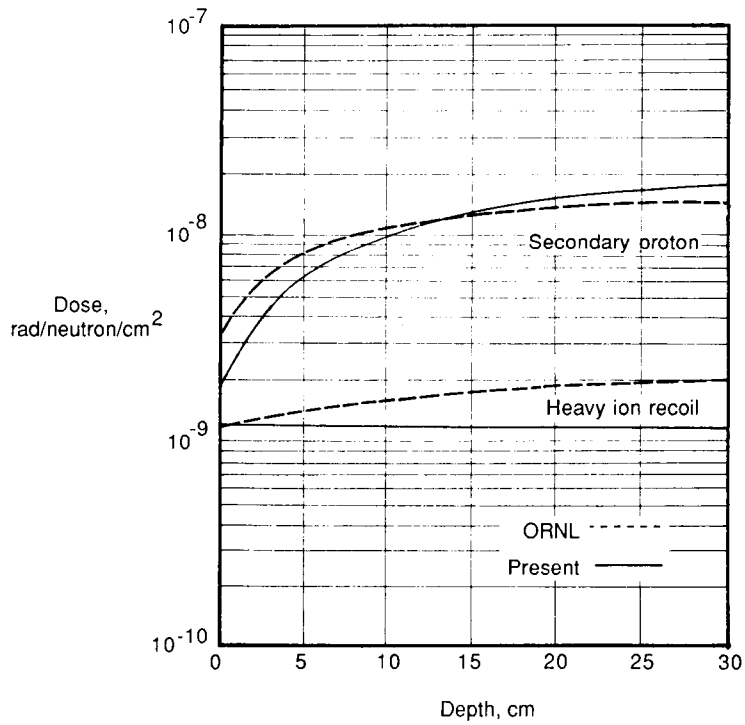

Figure 27. Dose in tissue due to normal incident 200 MeV neutrons according to reference 37 and present code.

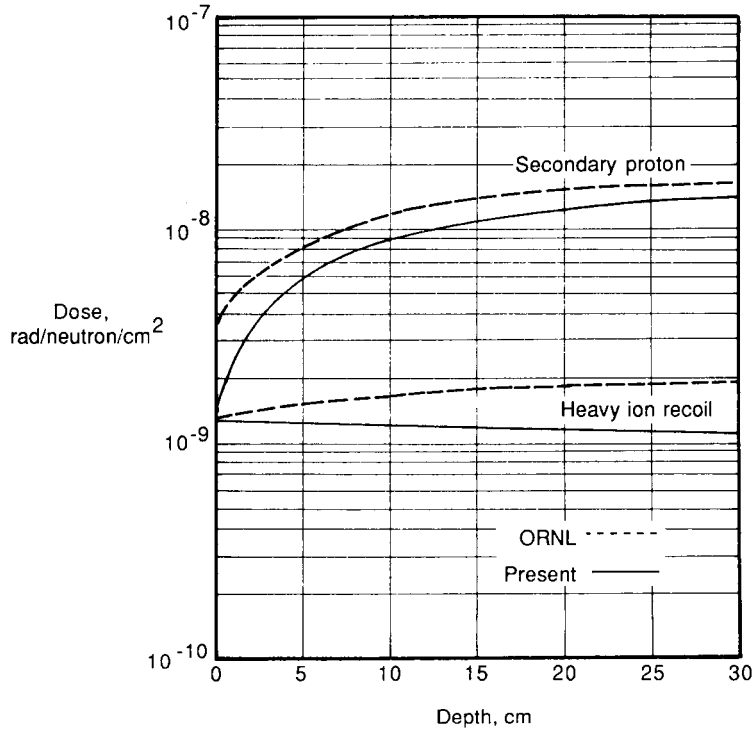

Figure 28. Dose in tissue due to normal incident 300 MeV neutrons according to reference 37 and present code.

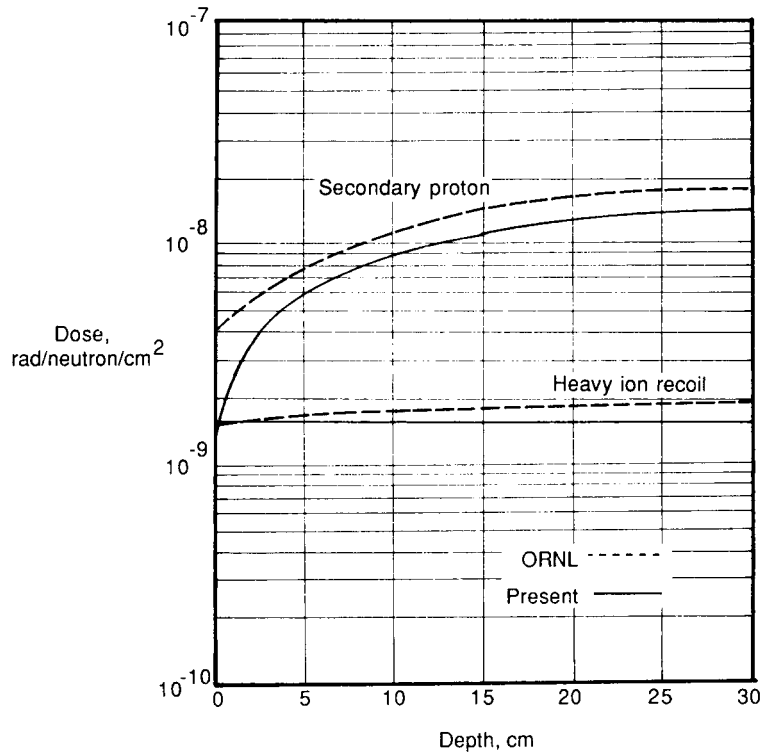

Figure 29. Dose in tissue due to normal incident 400 MeV neutrons according to reference 37 and present code.

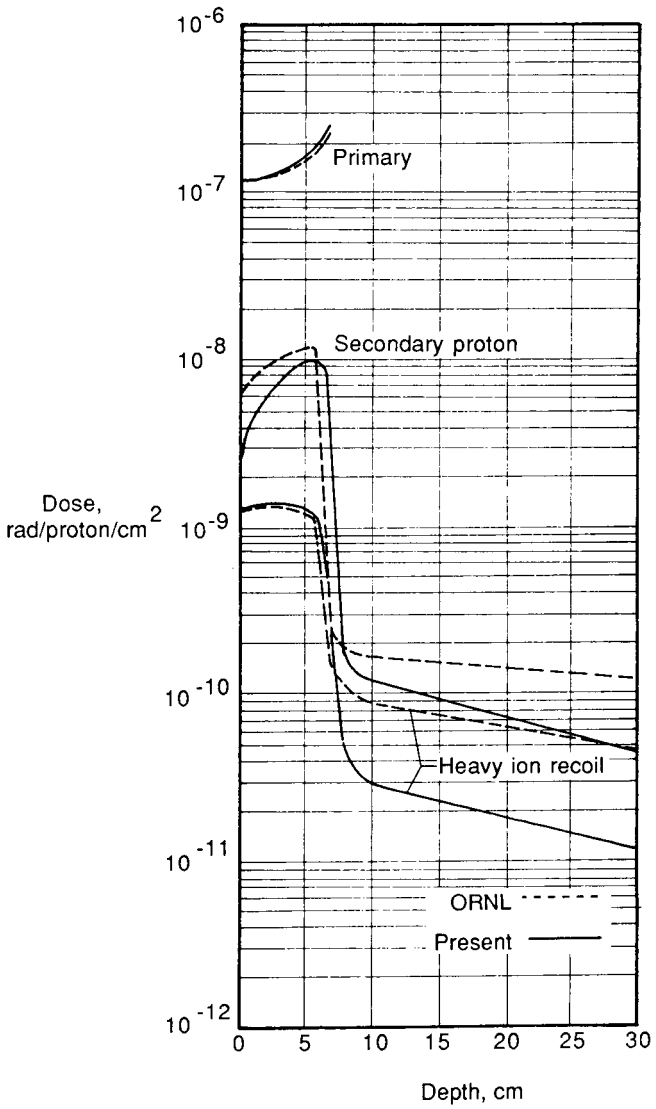

Figure 30. Dose in tissue due to normal incident 100 MeV protons according to reference 37 and present code.

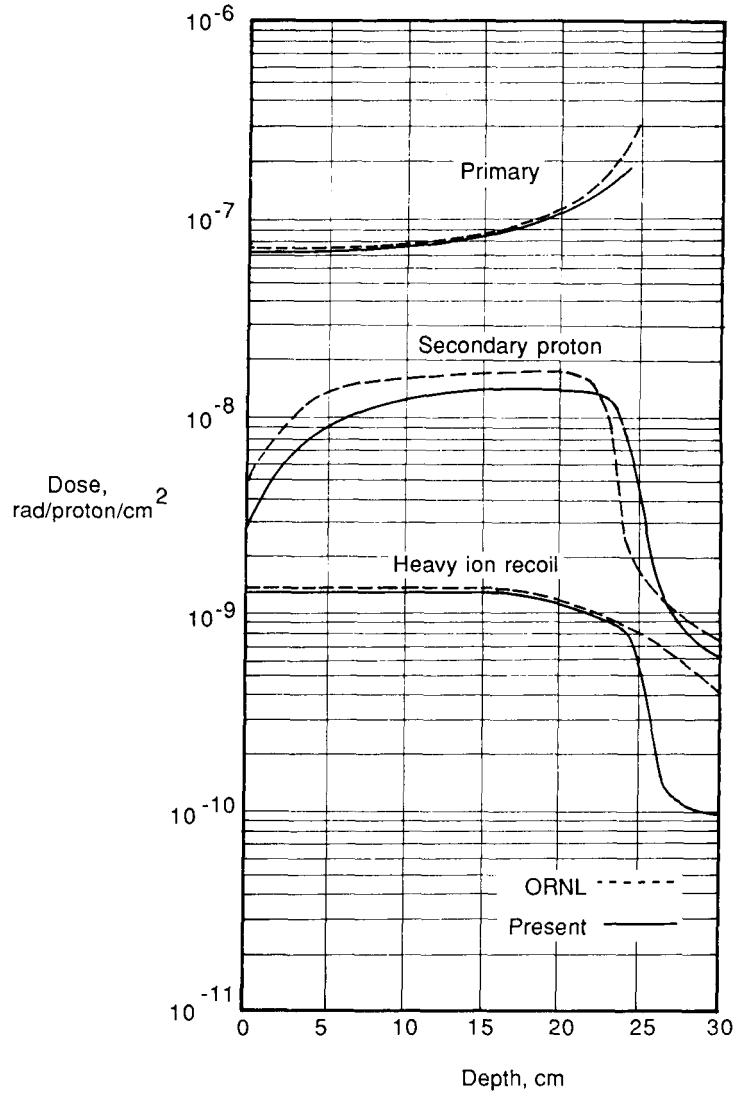

Figure 31. Dose in tissue due to normal incident 200 Mev protons according to reference 37 and present code.

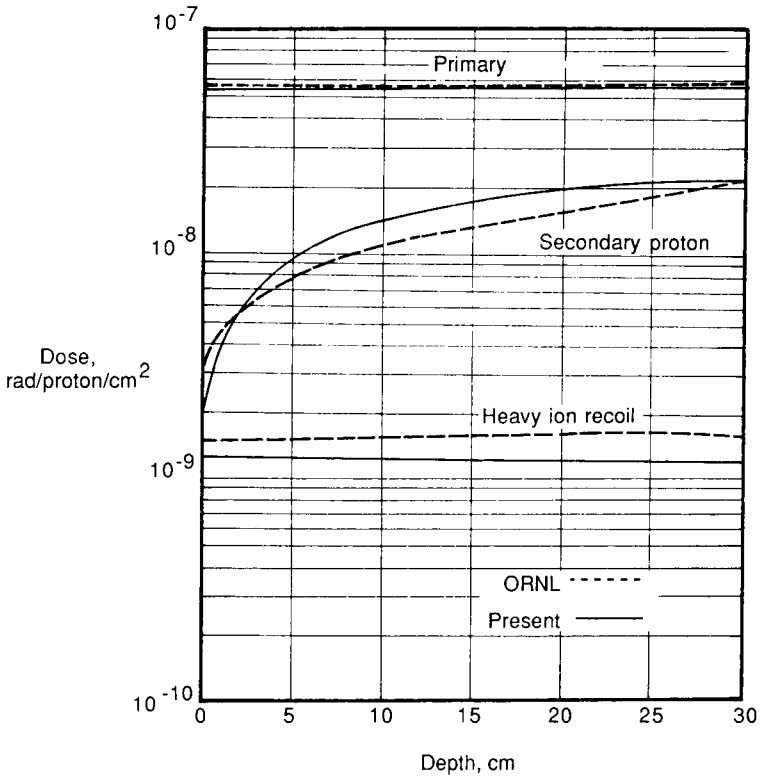

Figure 32. Dose in tissue due to normal incident 300 MeV protons according to reference 37 and present code.

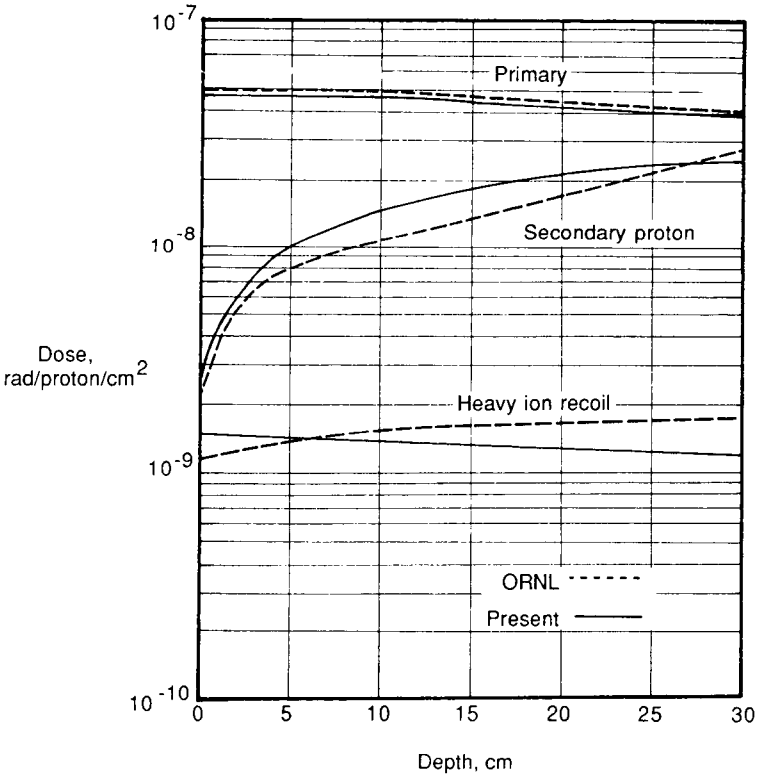

Figure 33. Dose in tissue due to normal incident 400 MeV protons according to reference 37 and present code.

NASA
National Aeronautics and Space Administration

Report Documentation Page

1. Report No.	2. Government Accession No.	3. Recipient's Catalog No.
NASA TM-4037		

4. Title and Subtitle	5. Report Date
BRYNTRN: A Baryon Transport Computer Code—Computation Procedures and Data Base	June 1988
	6. Performing Organization Code
7. Author(s)	8. Performing Organization Report No.
John W. Wilson, Lawrence W. Townsend, Sang Y. Chun, Warren W. Buck, Ferdous Khan, and Frank Cucinotta	L-16432
	10. Work Unit No.
9. Performing Organization Name and Address	199-22-76-01
NASA Langley Research Center Hampton, VA 23665-5225	11. Contract or Grant No.
	13. Type of Report and Period Covered
12. Sponsoring Agency Name and Address	Technical Memorandum
National Aeronautics and Space Administration Washington, DC 20546-0001	14. Sponsoring Agency Code

15. Supplementary Notes

John W. Wilson and Lawrence W. Townsend: Langley Research Center, Hampton, Virginia.
Sang Y. Chun and Warren W. Buck: Hampton University, Hampton, Virginia.
Ferdous Khan and Frank Cucinotta: Old Dominion University, Norfolk, Virginia.

16. Abstract

The present report describes the development of an interaction data base and a numerical solution to the transport of baryons through an arbitrary shield material based on a straight ahead approximation of the Boltzmann equation. The code is most accurate for continuous energy boundary values but gives reasonable results for discrete spectra at the boundary with even a relatively coarse energy grid (30 points) and large spatial increments (1 cm in H_2O).

17. Key Words (Suggested by Authors(s))	18. Distribution Statement
Space radiation Shielding Nuclear reaction	Unclassified—Unlimited Subject Category 93

19. Security Classif.(of this report)	20. Security Classif.(of this page)	21. No. of Pages	22. Price
Unclassified	Unclassified	42	A03

For sale by the National Technical Information Service, Springfield, Virginia 22161-2171